Bioactive Materials 11 (2022) 166–180

Contents lists available at ScienceDirect

Bioactive Materials

journal homepage: www.keaipublishing.com/en/journals/bioactive-materials

Surface processing for iron-based degradable alloys: A preliminary study on the importance of acid pickling

Letícia Marin de Andrade [a], Carlo Paternoster [a], Pascale Chevallier [a], Sofia Gambaro [a,b], Paolo Mengucci [c], Diego Mantovani [a,*]

[a] Laboratory for Biomaterials and Bioengineering, Canada Research Chair I in Biomaterials and Bioengineering for the Innovation in Surgery, Department of Min-Met-Materials Engineering, Research Center of CHU de Quebec, Division of Regenerative Medicine, Laval University, Quebec City, QC, G1V 0A6, Canada
[b] National Research Council, Institute of Condensed Matter Chemistry and Technologies for Energy CNR-ICMATE, Genoa, 16149, Italy
[c] Polytechnic University of Marche, Ancona, 60121, Italy

ARTICLE INFO

Keywords:
Biodegradable metals
Iron-based alloys
Acid pickling
Surface finishing
Pre-treatment

ABSTRACT

The formation of a heterogeneous oxidized layer, also called scale, on metallic surfaces is widely recognized as a rapid manufacturing event for metals and their alloys. Partial or total removal of the scale represents a mandatory integrated step for the industrial fabrication processes of medical devices. For biodegradable metals, acid pickling has already been reported as a preliminary surface preparation given further processes, such as electropolishing. Unfortunately, biodegradable medical prototypes presented discrepancies concerning acid pickling studies based on samples with less complex geometry (e.g., non-uniform scale removal and rougher surface). Indeed, this translational knowledge lacks a detailed investigation on this process, deep characterization of treated surfaces properties, as well as a comprehensive discussion of the involved mechanisms. In this study, the effects of different acidic media (HCl, HNO_3, H_3PO_4, CH_3COOH, H_2SO_4 and HF), maintained at different temperatures (21 and 60 °C) for various exposition time (15–240 s), on the chemical composition and surface properties of a Fe–13Mn-1.2C biodegradable alloy were investigated. Changes in mass loss, morphology and wettability evidenced the combined effect of temperature and time for all conditions. Pickling in HCl and HF solutions favor mass loss (0.03–0.1 g/cm^2) and effectively remove the initial scale.

1. Introduction

Metallic biodegradable alloys, also called *bioabsorbable alloys*, provide a new insight for a number of medical applications, including orthopedic, cardiac, and even dentistry [1]. In this context, Fe–Mn–C austenitic steels have been already reported as a valid alternative to Mg-based alloys for vascular applications [2,3]. Due to their outstanding mechanical properties, e.g. high ductility (deformation at rupture, A ≈ 20%) and strength (yielding strength, $\sigma_Y \approx 620$ MPa) [4,5], and their appropriate corrosion behavior (0.13 ± 0.01 to 0.24 ± 0.03 mm/year) [6,7], this new class of alloys is particularly attractive for thinner implants [8], such as stents, as they present more favorable mechanical properties than those of Mg-based ones [9].

Thermomechanical processing of alloys, comprising laser cutting [10], can be responsible for the formation of a relatively thick surface scale, presenting cracks, inclusions, chemical inhomogeneity, etc. In addition, also laser processing can generate debris and slag affecting the biomaterial surface finishing [11].

On the other side, the presence of a thin oxide layer on the metal surface is due to specific processes (for example electropolishing), creating a surface with features totally different from those properly attributed to the previously mentioned «scale». The thermomechanical scale is never accepted for applications requiring a strict control of the surface properties, because the oxide scale does not constitute an acceptable base for following applications; on the other side, the thin oxide scale, when carefully produced under strict procedures, could improve the material behavior, properties and interaction with the environment.

Thus, the removal of the thermomechanical scale, is mandatory for guaranteeing the removal of extrinsic and intrinsic contaminants, and to assure the good outcome of the following treatments (for example electropolishing or plasma treatments, etc.) In fact, the oxide scale could

Peer review under responsibility of KeAi Communications Co., Ltd.
* Corresponding author.
E-mail addresses: diego.mantovani@gmn.ulaval.ca, diego.mantovani@gmn.ulaval.ca (D. Mantovani).

https://doi.org/10.1016/j.bioactmat.2021.09.026
Received 21 October 2020; Received in revised form 4 September 2021; Accepted 20 September 2021
Available online 29 September 2021

interfere with the electrochemical, mechanical and cytocompatibility metal behavior, which is not acceptable for biomedical and other critical applications, such as, semiconductor and pharmaceutical [12].

The surface properties of metallic materials are fundamental for biomedical applications as the environment/surface interface plays a key-role in corrosion processes, cytocompatibility and triggering of fatigue phenomena [13–15]. Surface modification is often reported as an implant treatment that can occur in several step, each one taking into account a specific surface feature. Chemical and electrochemical treatment is essential especially for products and implants whose complex geometry could be compromised if any other kind of traditional treatment, such as mechanical polishing, is applied.

In particular, acid pickling, or *chemical descaling*, is a well-known technique that allows the removal of heat-formed scale from steel surfaces and extrinsic surface contaminants [16]. Pickling is interesting in terms of enabling a clean surface to facilitate subsequent treatments, such as galvanization or other chemical surface modification processes [17]. Acid pickling is based on the immersion of the oxidized sample in aqueous acidic solution [18]. However, the effectiveness of the oxide scale dissolution was strongly correlated to medium pH [19], acidic solution strength (pK_a) and chemical composition. For instance, an acid with high dissociation strength, $pK_a < -2$ [20], leads to a large amount of protons responsible for the dissolution of iron at the oxide/metal interface. This dissolution culminates in the detachment of the oxide layer from the substrate. However, the oxide scale solubility is affected by the acidic solution temperature, as the acid dissociation constant (K_a) varies in function of this parameter. Indeed, at higher temperatures, the acid ability to dissociate decreases, reducing the number of protons or its ability to form hydronium (H_3O^+) ions. The parameters to pickle a specific type of steel are also dependent on its composition as well as the state of the oxide scale. Therefore, pickling is a complex multi-parametric process, where solution composition, temperature and immersion time need to be finely tuned to the metallic substrate and its oxide state. In biomaterials, acid pickling was mainly investigated as pre-treatment to hinders corrosion, improve surface energy or create an oxide/hydroxide layer [21]. This technique is mainly used for alloys employed in permanent implants for blood contact applications, including stents, such as stainless steel 316L and Cr–Co, but also for Ti-based alloys mainly used in orthopedics [22,23]. For example, for 316LVM stainless steel stents, the influence of solution composition and immersion time on the material surface features was reported [24,25]. A mixture of 3% HF, 20–25% HNO_3 and deionized water at 35–40 °C was found to improve both surface finishing and mechanical integrity of the final device, by controlling its mass loss. Moreover, these media combined with the use of an ultrasonic bath, allowed the removal of all the contaminants and scale from the device surface after 10–40 min of immersion. Nevertheless, the same process for absorbable biomedical alloys may cause excessive mass loss, undesirable features and modify the mechanical integrity of the device [26]. Hermawan et Mantovani [27] already studied a pickling process to remove burrs and slags from the surface of a Fe–35Mn biodegradable stent. After-laser cutting, the material was immersed in a medium composed of 5% H_3PO_4 + 0.5% H_2O_2 + water solution (vol/vol) at 60 °C for 30 and 60 s, under sonication. This pickling setup enabled the elimination of the oxides formed during machining. However, a final porous surface similar to that found after annealing was obtained, indicating an over-pickling or the preferential dissolution of an alloy component, leaving a Mn-depleted layer. Indeed, corrosion inhibitors are widely used in industry to control over-pickling and corrosion rate [28]. Organic compounds containing heteroatoms such as oxygen, sulfur or phosphorus were found to be effective to reduce the corrosion rate of metallic materials [29]. Therefore, a process to control the dissolution of the oxide scale, and to remove contaminants from Fe–Mn–C biodegradable materials without attenuating mechanical integrity needs to be developed. The removal of this oxide layer or, at least, the control of its characteristics making the surface condition reproducible, in order to obtain specific surface properties for biomedical application, must be investigated. Thus, this work aimed at developing an acid pickling process as pre-treatment for further surface modification for Fe–Mn–C biodegradable alloys attaining an effective removal of the native oxide layer and a homogeneous chemical composition and surface morphology. In the current investigation, several pickling parameters, including the acidic solution composition, temperature and immersion time were considered and their effect on the tested samples evaluated.

2. Materials and methods

2.1. Materials

Hot rolled steel plates in the annealed, quenched and austenitic state of Fe–13Mn-1.2C (ISO GX120Mn13) named Hadfield were supplied by Polstar Metals Inc. (Canada). Coupons of 10 mm × 10 mm x 1 mm were cut for characterization after acid pickling. The nominal chemical composition of Fe–13Mn-1.2C alloy is reported in Table 1.

2.2. Pickling procedure

Samples were cleaned in two steps: (1) with an industrial non-acid blue cleanser (Diversey™, Canada) to remove grease, oils and other impurities accumulated on the surface; and (2) with acetone and methanol in an ultrasonic bath for 5 min each. After the cleaning, samples were rinsed with acetone and then dried with filtered compressed air. The samples were then stored under vacuum until further use. Six commercial acidic solutions supplied by Laboratoire MAT (Canada) and VWR™ chemicals (USA) were used to pickle the samples and are listed in Table 2. Two main parameters, known to strongly impact the pickling efficiency, have also been considered: the immersion time (t), and the temperature (T). Times from 15 s to 240 s, and bath temperatures at 21 °C ± 0.4 °C and 60 °C ± 0.5 °C were selected based on previous studies [17,18] that observed a high efficiency on the removal of the scale due to the increasing of dissolution by increasing the time and temperature [30]. The chosen range of temperature was settle following the recommendation of the ASTM A380/A380M − 13 [17] and the exposition time was selected based on the pickling treatment on biodegradable Mg-based alloys [21,31].

Samples were immersed in the acidic bath, for the chosen time and at the selected temperature, then rinsed with acetone and dried with filtered compressed air. Before characterization, they were stocked in a desiccator with a vacuum level of 30 Torr at room temperature until further use. The complete set of experiments is summarized in Table 2. The sample name is based on the treatment condition, meaning acidic solution composition, immersion temperature and treatment duration. For instance, the sample named 1CRT30 corresponds to an immersion in hydrochloric acid, HCl (1C), at room temperature (RT) for 30 s (30). On the basis of the set of experiments, only the most relevant data evidencing the effect of the studied parameters on mass loss, topography, roughness and chemical composition of the surface were presented. For these reasons, the samples tested at different times (e.g 15 s and 240 s) are not listed in Table 2, while their mass loss results appear in the following section. The media used in the present work are commercial ACS grade solutions (Lab Mat, Québec, QC Canada) corresponding, in volume, to HCl (36%), HNO_3 (67–70%), H_3PO_4 (85%), CH_3COOH (99.5%), H_2SO_4 (96%) and HF (48%).

Table 1
Nominal chemical composition of Fe–13Mn-1.2C alloy.

Element	C	Mn	Si	S	P	Fe
Composition (wt.%)	1.0–1.3	12–14	0.2–0.4	<0.02	<0.035	bal.

Table 2
List of sample names.

Acid solution	Simplified samples name	Extended samples name			
		Temperature 21 °C		Temperature 60 °C	
		30 s	60 s	30 s	60 s
HCl	1C	1CRT30	1CRT60	1C6030	1C6060
HNO_3	2 N	2NRT30	2NRT60	2N6030	2N6060
H_3PO_4	3P	3PRT30	3PRT60	3P6030	3P6060
CH_3COOH	4A	4ART30	4ART60	4A6030	4A6060
H_2SO_4	5S	5SRT30	5SRT60	5S6030	5S6060
HF	6F	6FRT30	6FRT60	6F6030	6F6060

2.3. Characterization

The samples were weighed before and after pickling with a 5-digit precision digital balance (Analytical Plus–Ohaus, USA) to evaluate the evolution of descaling fraction when increasing time and temperature. Five samples per condition were evaluated and their mass loss (W_L) was calculated according to Eq. (1):

$$W_L = \frac{(W_0 - W_f)}{S} \quad (1)$$

where W_0 and W_f are the weights (g) measured before and after pickling, respectively, while S is the total area of the samples, considered as ~ 2.2 cm^2.

Surface topography and roughness were evaluated by using a Dektak XT stylus profilometer equipment (Veeco-Bruker, USA) with a 12.5 μm diameter stylus and an applied force of 1 mg. Six linear scans, each of 2 mm, were carried out for each condition wherein the roughness (R_a) was calculated by following Eq. (2):

$$R_a = \frac{1}{l}\int_0^l |y(x)|dx \quad (2)$$

where R_a is the measured roughness (μm), l is the measured length (mm), and |y(x)| is the deviation of the absolute values of the profile heights over the evaluated length (μm).

Wettability response of the surfaces was determined by static contact angle measurements using a camera system (VCA 2500 XE, AST Products Inc., USA), according to ASTM-D749 [32]. The analyses were carried out at 25 °C, with 1 μL ultrapure water droplets. The contact angle measurements were performed in five different regions per sample for each studied condition.

Topographical changes induced by pickling treatments on Fe–Mn–C alloy surface were assessed by the use of a FEI Quanta 250 scanning electron microscope (SEM) from Thermo-Fisher (USA). SEM images were acquired with an acceleration voltage of 15 kV. The microscope is equipped with an energy dispersive X-ray spectrometer (EDS) for microanalysis system EDAX AMETEK Material Analysis (USA). The EDS analyses were performed at 20 kV to determine the surface chemical composition as well as the elemental distribution by map scanning.

X-ray photoelectron spectroscopy (XPS) measurements were assessed by a PHI 5600-ci spectrometer (Physical Electronics, USA). A standard aluminum X-ray source (1486.6 eV) was used to record survey spectra, while high-resolution spectra of C1s and O1s regions were recorded with a Mg K_α X-ray source (E = 1253.6 eV), both without charge compensation. Detection was carried out at 45° angle with respect to the normal surface, and the analyzed area was 0.5 mm^2. A curve fitting procedure was performed by means of a least-squares minimization procedure employing Gaussian–Lorentzian functions, followed by the subtraction of a Shirley-type background. The C1s peaks were referenced at 285 eV (C–C and C–H).

All numerical data were analyzed by ANOVA and followed by Tukey test for specific comparisons between mean values. Results were expressed as *(mean value) ± (standard deviation, SD)*. If probability values for a set of data were found to be < 0.05 ($p < 0.05$), the differences were considered statistically significant.

The as-received (AS-REC) condition, also addressed as "cleaned", was studied and characterized with the different techniques aforementioned in order to evaluate the surfaces properties from different points of view. Prior to the cross-section SEM images, samples were mechanically polished with SiC abrasive papers of 180 and 320 grit. Sample surfaces were observed without any special treatment: specimens were mounted on an aluminum stub and were used to put in evidence the features of the oxidized layer. For phase identification, X-Ray diffraction (XRD) analyses were performed in a Bruker D8 Advance ECO diffractometer with Cu-Kα radiation (40 kV of voltage and 25 mA of current) with a step size of 0.02°. MAUD (Material Analysis Using Diffraction, http://maud.radiographema.com/) software was used for peak identification.

3. Results

3.1. Mass loss

The oxide scale removability was studied by assessing the mass loss of the samples after pickling in the six acidic solutions (Table 1). Results are presented in the graphs of Fig. 1, where the mass loss (g/cm^2) was expressed as a function of the temperature.

The amount of removed scale appeared to be correlated to the pickling parameters, as expected. Indeed, the 1C, 4A and 6F samples clearly presented a significant variation of the mass loss in function of both time and temperature, with a respective maximum mass loss of 0.089 g/cm^2, 0.001 g/cm^2 and 0.03 g/cm^2 at 60 °C for 240 s. The mass loss values are mainly associated to the scale removal, but the pickling medium may reach the substrate and metal dissolution can take place. Strong acidic solutions, such as HCl and HF, are known to rapidly lead to steel substrate dissolution compared the other acidic solutions for the same time and temperature [23]. Indeed, a graphical representation of mass loss in a long-time scale may present a discernible trendline break, which can be associated to the difference in the dissolution of the scale and the metal [33]. Therefore, this event was clearly observed for all the solutions, except for 3P in both temperatures mainly due to the high standard deviation calculated for conditions from 15 to 120 s. Briefly, the interval observed for each solution was: 1C [100–120 s] for 21 °C and 60 °C, 2 N [100–120 s] for 60 °C, 4A [15–30 s] for 21 °C and [15–60 s] for 60 °C, 5S after 30 s for 21 °C and 15 s for 60 °C, and finally 6F [100–120 s] for 60 °C. Hence, the conditions showing this event revealed a beginning of over-pickling by the end of this interval, meaning that metallic compounds from the substrate are being removed. To support these findings, the chemical composition and the phases of the scale was studied by EDS mapping and XRD in order to validate and compare if the mass loss found in these intervals corresponded to the expected calculated mass loss of the scale. These results are presented in the next section (3.2).

Moreover, in contrast with the results aforementioned, negative values indicating a mass increase were observed for 2 N, 3P and 4 A, after 15 s of immersion, in agreement with the literature [34,35].

3.2. Chemical composition of the scale

Fig. 2 displays the cross-section morphology, as well as the elemental mapping and X-ray diffraction analyses performed for the AS-REC condition. Elemental mapping at the interface between the oxide scale and the metallic substrate (Fe–13Mn-1.2C) was performed (Fig. 2) for carbon, oxygen, iron and manganese to the same cross-sectional area than Fig. 2 a.

The scale thickness of the various cross-section images varied in the range 5 ÷ 100 μm. An oxide layer composed of compact pieces of scale of different sizes, featuring voids, cracks and pores was observed (Fig. 1a).

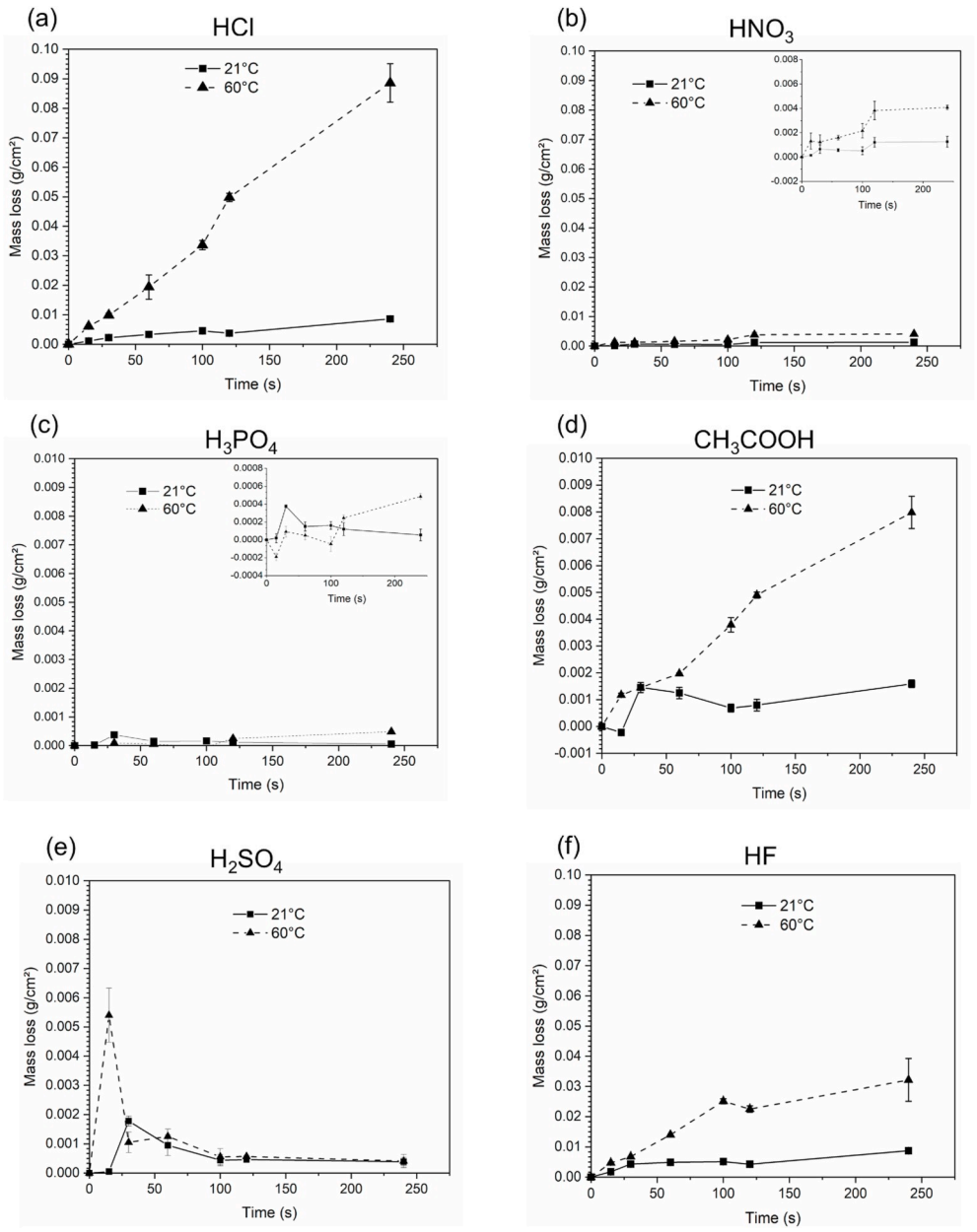

Fig. 1. Mass loss (g/cm^2) of samples after acid pickling in six different acidic solutions at 21 °C and 60 °C, as a function of time.

Cleaned samples presented a spalled surface: this is often observed at the interface of oxide layer/substrate after thermal treatment [36]. Fig. 2 b shows XRD patterns for the as-received condition. Four phases were detected: metallic iron, $Mn_{0.43}Fe_{2.57}O_4$, $(FeO)_{0.664}(MnO)_{0.336}$ and Fe_2O_3, hematite. With these findings, it was possible to calculate the theoretical density, the mass and the volume of the oxide layer, that means ρ_{oxi} = 5.94 g/cm^3, m_{oxi} = 0.006 g and v_{oxi} = 1% of the total volume, respectively. The volume and the mass values found for the oxide layer were used to compared the mass loss observed for different conditions presented in the previous section.

From EDS mapping, Fig. 2(c–f), the percentage of each element was detected as O (24%), C (44%), Fe (30%) and Mn (2%). A noticeable Mn-depletion was observed in Fig. 2 f. An interesting observation is that Mn-depletion zones are similar to Cr depletion ones found at the interface of oxides and stainless steels substrates, which could affect the descaling process and the corrosion resistance of the alloy [37,38]. A lower Mn amount at the interface between the oxide and the bulk material was already reported [39–41], as well as the kinetics of internal oxidation of Mn-steel alloys [42]. Manganese depletion causes phase transformation from austenite to ferrite, as a function of the amount of atmospheric oxygen and the temperature [43]. Oxygen and manganese diffuse faster in ferrite than in austenite, increasing the precipitation of MnO [42]. Indeed, the presence of the manganese oxide is supported by XRD analyses.

3.3. Surface topography and roughness

The surface topography and roughness analyses were carried out for samples immersed in acidic solutions for 30 s and 60 s, at 21 °C and 60 °C. These conditions were chosen in function of previous results that showed the beginning of the intervals of dissolutions for no longer than 100 s, thereby indicating the possibility of over-pickling on the surface from that time.

Surface topography and roughness (R_a) were assessed by stylus profilometry to evaluate the smoothness and homogeneity of the acid pickling conditions. Six measurements were performed on random areas

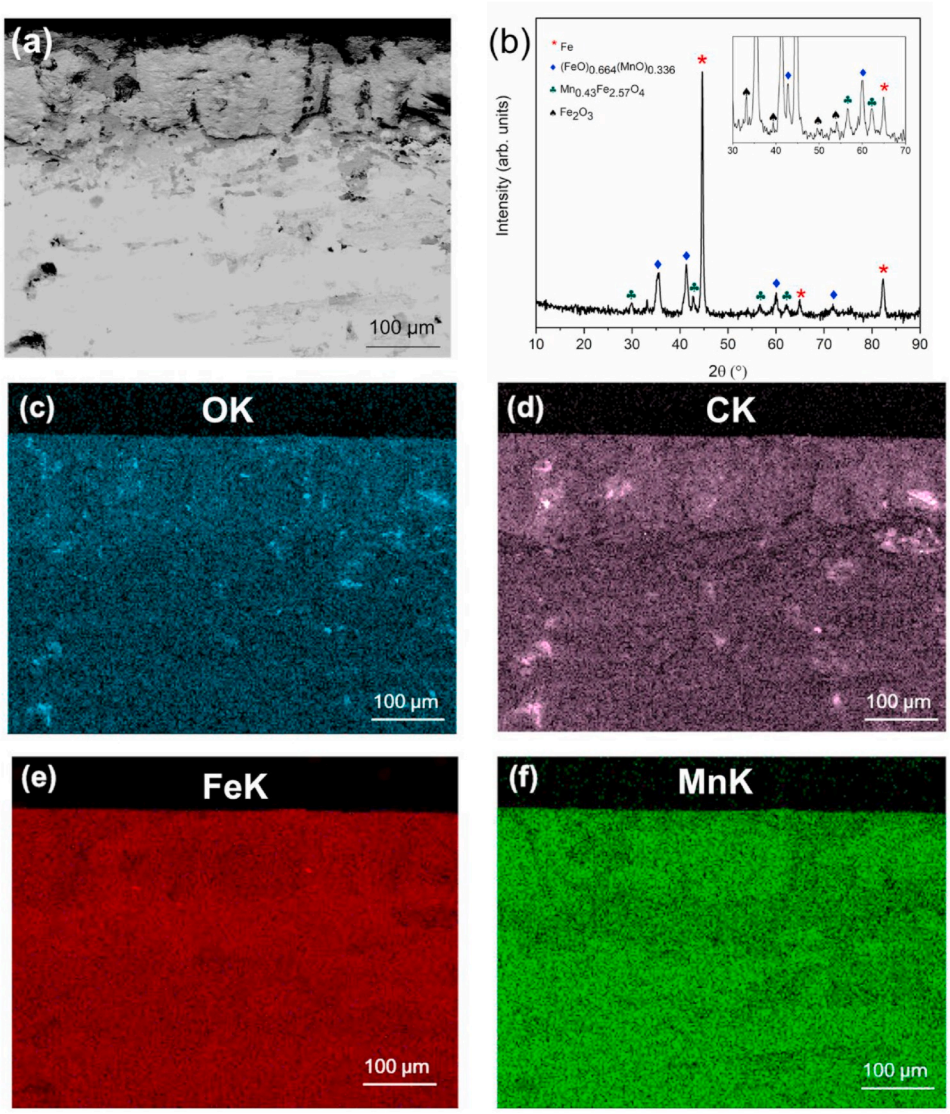

Fig. 2. (a) Cross-section of an untreated sample (b) XRD patterns of the scale surface and mapping of cross-section represented in (a), showing the amount of (c) oxygen, (d) carbon, (e) iron and (f) manganese.

on one sample for each condition, in order to assess the surface topography after pickling. The results were depicted in Fig. 3, displaying the roughness variation according to the temperature and pickling time for each used medium. At first, cleaned surface samples were characterized in order to compare the subsequent treatments with the initial condition, the roughness value $R_a = 1.08 \pm 0.20$ µm was found. At 21 °C (RT condition) no significant differences in term of roughness were observed for all the used media for 30 s of immersion. However, increasing the time to 60 s had an impact on the roughness. For this immersion duration, there was a significant difference between the 1CRT60 and 5SRT60 conditions with roughness values of 1.15 ± 0.20 µm and 0.77 ± 0.18 µm, respectively. Regarding the effect of treatment time, when pickling was performed at 21 °C, significant variations of roughness were noticed for 6FRT30 (1.33 ± 0.45 µm), 3PRT60 (0.78 ± 0.10 µm), 5SRT60 (0.77 ± 0.18 µm) conditions. The low roughness observed for 3P samples at room temperature was not expected, since at temperatures higher than 40 °C, phosphate-rich solutions are in general known to promote phosphatization reactions instead of removing the oxide layer [44,45]. A high reactivity of phosphoric solutions for native oxide removal has been demonstrated to occur in temperature ranges varying between 20 and 50 °C [46]. However, the Tukey test used herein did not exhibit any significant variation in roughness values between samples when treated at 21 °C or at 60 °C. Furthermore, no significant difference was found for all conditions when pickling immersion was performed at 60 °C.

3.4. Wettability behavior

Morphology, roughness, chemical composition and surface charges may lead to changes in surface tension, normally represented by surface wettability. Fig. 4 exhibits the contact angle (CA) values assessed for samples after the pickling treatment.

In particular, AS-REC samples exhibited a moderately hydrophilic behavior (59° ± 11°), which was also found for other conditions, for example 4A both at 21 °C and 60 °C after 60 s (4ART60: 71° ± 6°; 4A6060: 65° ± 11°) and for 5S for 30 and 60 s at 60 °C (5S6030: 33° ± 7°; 5S6060: 64° ± 10°). In particular, for 5S, at 60 °C after 30 s exposition the most hydrophilic response among all conditions was observed. From Fig. 4 and for statistical analyses followed by Tukey test, contact angle measurements, at 21 °C, exhibited significant differences among all conditions. 4A and 5S samples displayed opposite trends with time passing from 30 s to 60 s: an increase of hydrophilic behavior for the acetic solution (80°–61°, in this order), while the sulfuric solution exhibited a higher contact angle value (80°–131°) showing a highly hydrophobic character.

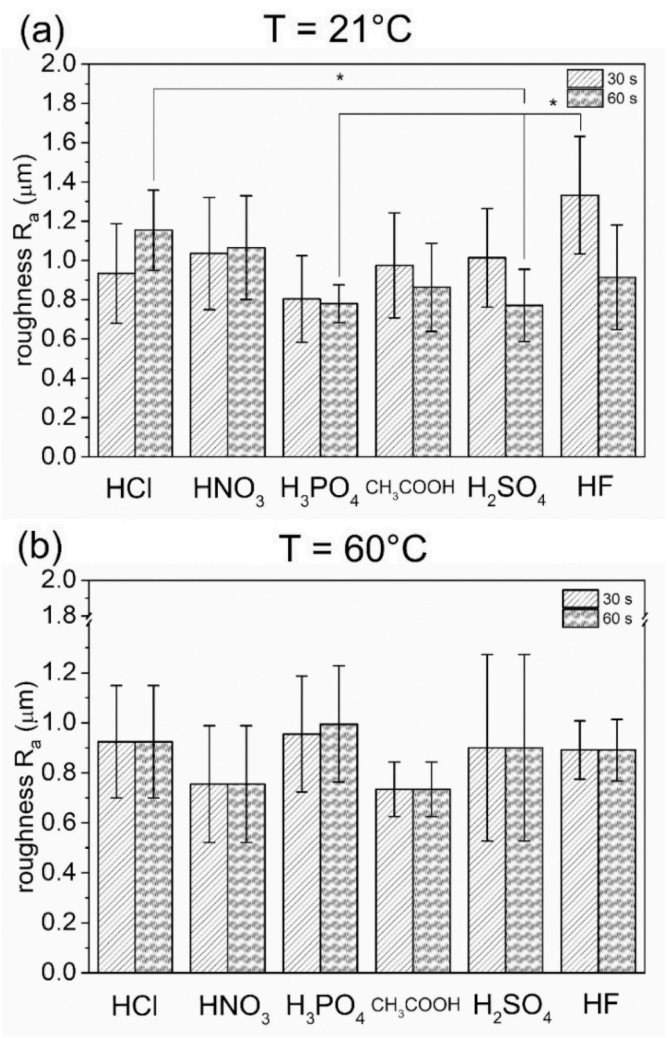

Fig. 3. Roughness measurement for samples after acid pickling at (a) 21 °C (RT) and (b) at 60 °C considering 30 and 60 s as immersion times. * Indicates there is a significant difference (p = 0.05) among the samples.

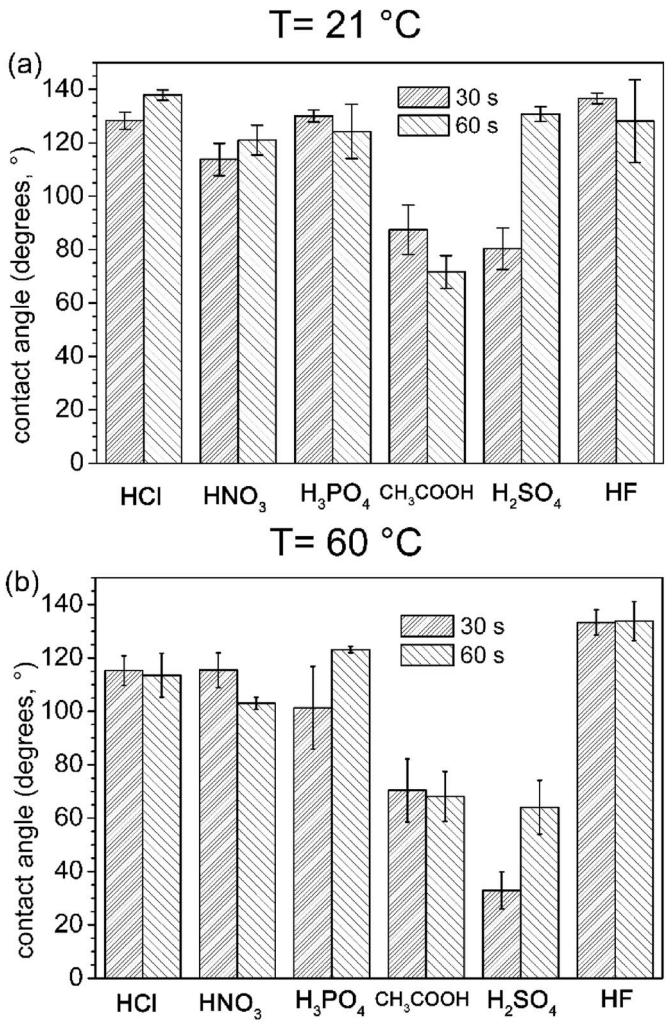

Fig. 4. The contact angle values of samples surface after acid pickling treatments at (a) 21 °C and (b) 60 °C, respectively, considering 30 s and 60 s as immersion times.

At 60 °C, the immersion time has no influence on wettability for 1C, 4A and 6F samples. Pickled samples in H_3PO_4 medium show the same behavior as observed for 21 °C. However, in H_2SO_4 after 30 s (5S6030 condition), surfaces presented the lowest contact angle (32° ± 7°) and, compared to samples treated in CH_3COOH for 60 s, both exhibited statistically the same contact angle values, 64° ± 10° (5S6030) and 68° ± 9° (4A6060), respectively. At 60 °C, 4A and 5S samples showed statistically the same behavior as the cleaned one.

In fact, one of the reasons for an oxidized surface exhibiting high surface energy, i.e. a low contact angle, is due to the presence of polar groups with oxygen-containing moieties such as hydroxyl (-OH) and carboxyl (-COOH) groups [47], which is also observed for surfaces cleaned with organic solvents, such as acetone and methanol [48]. However, surfaces after pickling processes mainly exhibited a hydrophobic behavior (90°< CA < 150°), sometimes approaching a super hydrophobic behavior (CA>150°). In literature, pickling has been generally shown to decrease the contact angle of metallic surfaces [49]. Examples included the study performed by Liu et al. that investigated an acid pickling pre-treatment of AISI 304 steel immersed in a solution of 15.3% HNO_3 + 2% HF + 82.7% H_2O (w %). In this work, samples without any treatment exhibited a contact angle of 79°; after acid pickling, a decrease was noticed and a contact angle of 65° was found. Nevertheless, in a recent study aiming to create a super-hydrophobic surface, an acid pickling procedure with phosphoric acidic solution at 55 °C for 2 min was applied to AISI 304 austenitic steel. After the pickling treatment, a contact angle of 98° ± 9° and a roughness (R_a) of 6.1 μm were obtained [50]. The hydrophobic behavior could be explained by Cassie-Baxter theory, which shows that a hydrophobic surface behavior is caused by the chemically and morphologically heterogeneity [51]. For some conditions studied in the present work, the high variation of roughness observed (Fig. 3) may influence their higher contact angles measured (e.g, 6FRT30 condition, CA = 137° ± 2° and a R_a = 1.33 ± 0.45 μm).

3.5. Surface morphology after acid pickling

SEM images reported in Fig. 5 show the main features of the treated sample surfaces. After almost all the pickling conditions, cavities and porous structures were observed. These features could be attributed to some residuals of the previous oxide layer (see for example Fig. 5 b.3); other precipitation structures could also form due to the reaction of the substrate alloy (for example in the case of Fig. 5 b.5, b.7, c.1) with the used medium. The presence of various particles was found and attributed to adventitious contaminations (Fig. 5 d.1 and d.3). While assessing the surface morphology of Fig. 5 a.1, a.7, b. 3, b.7, it was evident that not all the conditions resulted in a scale removal process providing a final homogeneous topography. For example, the microscope survey of a 2N6030 sample (Fig. 5 b.6) showed the presence of zones more severely

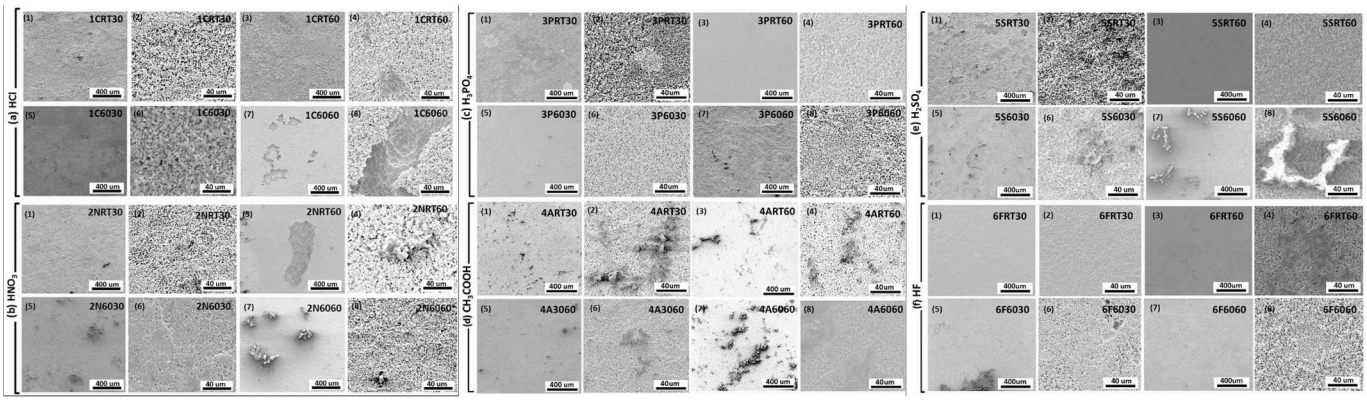

Fig. 5. Morphology and highlighted features of SEM pictures for pickling at 21 °C and 60 °C, varying with 30s and 60s time conditions in immersion at (a) HCl, (b) HNO_3, (c) H_3PO_4, (d) CH_3COOH, (e) H_2SO_4, (f) HF.

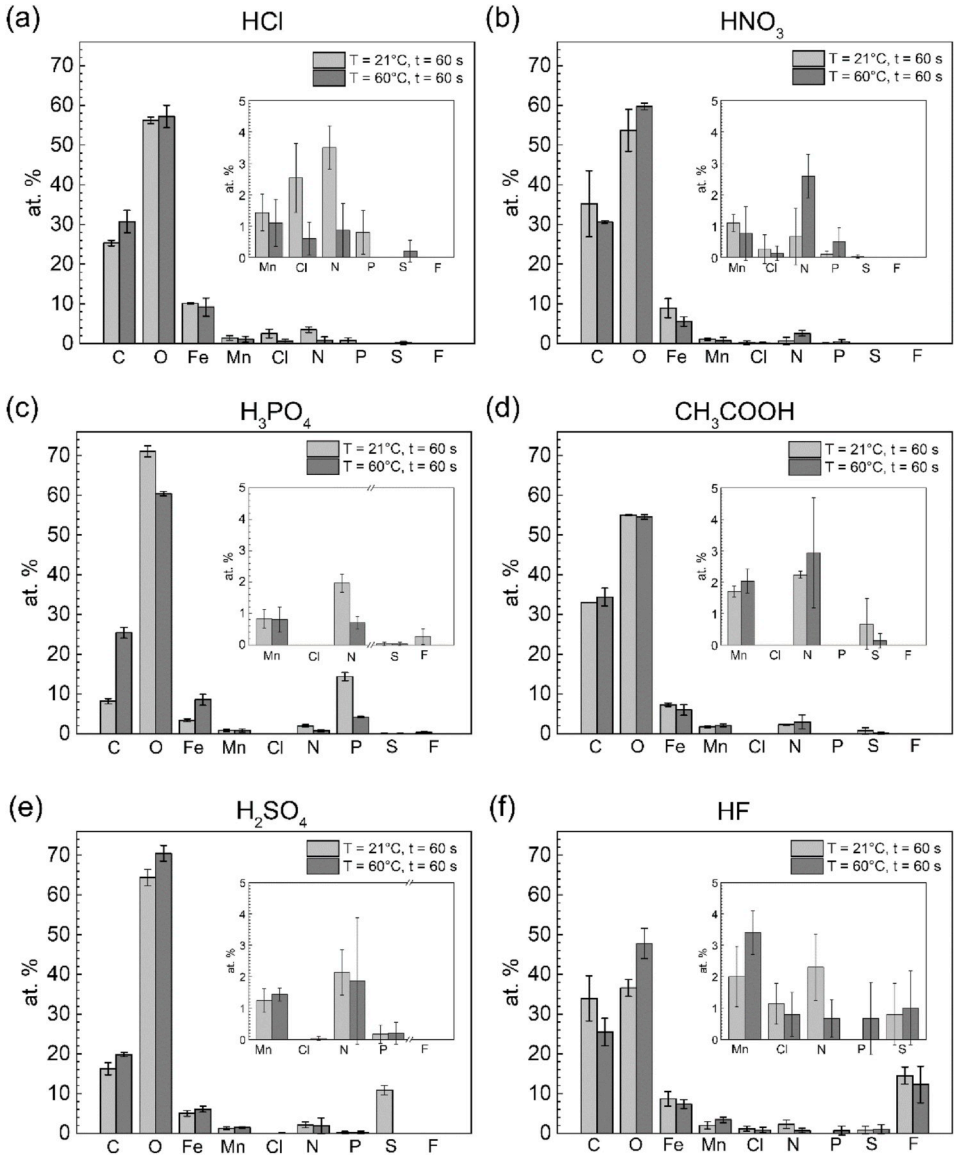

Fig. 6. XPS survey for (a) 1CRT and 1C60; (b) 2NRT and 2N60; (c) 3PRT and 3P60; (d) 4ART and 4A60; (e) 5SRT and 5S60; and (f) 6FRT and 6F60 after 60 s of immersion. The inlets show the amount of Mn, Cl, N, P, S and F, where needed, to describe the low amounts main elements found on the sample surfaces.

etched than others, resulting in plateaus and depressions. Nevertheless, the surface morphology after an exposition time of 60 s (2N6060) presents a more uniform featured surface. Some etching produced a more homogeneous and finer features than others, e.g. HF (Fig. 5 e.3-4 and f.1-2). No preferential etching patterns were observed, along the grain boundaries, or corresponding to other substrate features.

Fig. 5 a.8 evidenced the presence of a well-developed cellular morphology in the middle of the analyzed area of 1C6060 condition. Li et al. [23] described how the formation of these cells, often in the range of a few micrometers, began to appear at the start of pickling in HCl of a system composed of $Fe/Fe_2O_3/FeO/Fe_3O_4$ affects the corrosion potential and the morphology. This specific morphology, also found by other authors in literature, confirmed the dissolution mechanism of the discontinuous oxide layer in several acidic media [52].

3.6. Surface chemical characterization

3.6.1. XPS - surveys

XPS surveys were carried out for samples immersed in acidic solutions for 60 s, at 21 °C and 60 °C. These conditions were chosen in function of previous results that presented significant differences regarding the temperature influence such as mass loss and wettability. Furthermore, roughness evaluation showed significant influence for 60 s of pickling conditions. From XPS survey of AS-REC samples, C, O, Fe and Mn were found on the surface, with the following amounts: 47.2 ± 6.4 at. %, 42.6 ± 7.3 at. %, 6.4 ± 1.5 at. % and 2.8 ± 0.4 at. %, respectively. The surface composition of material can be different from that of the bulk material, due to the presence of surface species formed by interactions with the environment (oxides, hydroxides, adventitious carbon, etc.) [53].

Fe–13Mn-1.2C is in fact composed of Mn in the range of 11–14 wt % and C in the range 1.1–1.4 wt %. For calculation purposes, the nominal composition of the alloy was considered; the presence of impurities in the steel (Si, P, S, Cr, Ni, Cu, Mo, V, Ti and Al) was neglected. This hypothesis was consistent with the experimental measurements. The range of the considered Mn amount (wt. %) was between $Mn_{min} = 10.7$ at. % and $Mn_{max} = 13.5$ at. %. In particular, Mn_{min} corresponds to the minimum possible amount of Mn, with a maximum amount of Fe, while Mn_{max} is related to maximum amount of Mn, with a minimum amount of Fe. Then, the first ratio for the bulk alloy Fe_{max}/Mn_{min} is 8:1, while the second one, Fe_{min}/Mn_{max}, is 6:1. The mentioned ratios provide a range of reference for chemical compositions, typical of the material "bulk", which can be compared to the treated samples.

For 1CRT and 1C60 samples, the amount of O ≈ 55 at. % and C ≈ 30 at. % did not vary in any relevant way (Fig. 6). A slight increase in carbon was found for 1C60. The atomic ratio between Fe and Mn was 9:1 for 1CRT and 10:1 for 1C60, showing a surface enrichment of Fe, especially for the higher temperature condition. The decrease of Mn could be attributed to the scale removal and to the presence of the Mn-depleted layer normally found in this steel substrate [38], as mentioned above.

In certain cases, residual elements from the acidic solution were detected for the different investigated media: this was the case for example for fluorine from HF, sulfur from H_2SO_4, and phosphorus from H_3PO_4. The anions of each considered acid can form the corresponding salts on the surface of the studied alloy. Moreover, other elements in the form of impurities, such as N, S, P, F and Cl, were also detected. Their presence was attributed to the remaining scale on the steel surface, which is not only formed by mixed oxides, but also by compounds formed during the manipulation process (green rust, etc.)

For 2 N samples, the amounts of C (~55 at. %) and O (~30 at. %) did not change for treatments performed at 21 °C or 60 °C. Fe/Mn ratios were respectively 8:1 for 2NRT and 7:1 for 2N60, showing a high amount of Fe, closer to the higher limit for the bulk material. 3P sample surface showed ~14 at. % of P (when pickled at 21 °C while ~4.2 at. % for T = 60 °C). This higher percentage of P for RT samples (~14 at. %) was associated to the high amount of O (~70 at. %), and it could be related to the phosphate formation [54]. On the contrary, for P60 samples, O and P lower amounts (respectively, 60 and 4 at. %), and C higher percentage (25 at. %) were related to a lower formation of surface phosphates [54]. Fe/Mn was 4:1 for RT and 10:1 for T = 60 °C.

Even if different temperatures were used in the process, the use of CH_3COOH did not change the amounts of C, O, Fe and Mn in a relevant way, as they were respectively 35, 55, 6.5 and 2.0 at. %. More precisely, Fe/Mn ratio was in the range 4:1 (4ART) to 3:1 (4A60).

The presence of S was also detected for 5SRT: in particular, an amount of S of ~11 at. % was found. For this condition, the O amount was equal to 65 at. %, while C amount was 16 at. %. They increased respectively to 71 and to 20 at. % for 5S60. However, no significant amount of S was detected for 5S60, even if the Fe/Mn ratio was similar and equal to ~4:1 for both the investigated temperatures. For what concerns the pickling with HF, up to 15 at. % of F was detected for 6FRT, while it decreased to 12 at. % for 6F60. Surface C amount decreased with temperature from 34 to 26 at. %, whereas O increased from 37 to 48 at. %. Fe/Mn ratio was 5:1 for 6FRT and 2:1 for 6F60.

3.6.2. XPS high-resolution analyses

As already stated in the Materials and methods section, all the conditions were analyzed for the temperatures of 21 °C and 60 °C, each one for a duration of 60 s. For all the pickling conditions, all the C1s spectra showed a very deconvolution, even though slight differences were noticed. Indeed, they exhibited three main peaks, named for sake clarity as C1, C2 and C3 evidenced in Table 3. C1 was attributed to the presence of adventitious carbon, bound to carbon or hydrogen, that is C–C or C–H. C2 was attributed to the presence of C–O/N species, while C3 to the formation of R-O-C═O bounds [55,56]. However, their respective contributions changed depending on the initial acidic solution temperature as shown in Table 3. Indeed, at room temperature, C1 contribution varied from 65 to 75%, C2 from 10 to 15%, and C3 from 15 to 25%, whereas at 60 °C, their respective contributions ranged respectively from 45 to 70%, 15–35% and 10–20%. The acetic acid C1s HR spectrum was of particular interest, as it exhibited a high amount of C–O and C═O contributions, reaching 39 and 16%, respectively, with the lowest amount of C–C/C–H contribution (45%). This observation could possibly be associated to carbonyl from acetic acid reacting with the metallic surface.

The O1s high-resolution spectra (Fig. 7) of the different pickling conditions (1C, 4A and 6F) could be mainly deconvoluted in three energy bands, namely as O1, O2 and O3. These peaks correspond to the presence of oxygen as oxide (Me–O, O1), hydroxide (OH, O2) or physio-absorbed water (H_2O, O3) [57]. However, some shifts in their respective binding energy as well as in their relative percentage were observed (Table 3): for instance, O1 contribution ranged from 59 to 2%, O2 from 71 to 30%, and O3 from 24 to 9%. Even though these three bands were still present in 3P samples, for room temperature, an additional peak, O4, was found. This O4 band at 534.1 eV representing 6%, was normally attributed to adsorbed water [58]. This band was not detectable when the acidic pickling was performed in H_3PO_4 at 60 °C. Furthermore, the respective contributions of the other characteristic bands differed depending on the working temperature: from room temperature to 60 °C, O1 contribution increased from 2.4 to 39.4%, whereas O2 and O3 decreased from 67.1 to 53.2% and from 24.1 to 7.4%, respectively. Of particular interest, the high contribution of O2, 67.1% at room temperature, correlated to the 14 at. % of P detected in XPS survey spectra, is explained by the fact that this contribution may is not only due to Me–O–H, as stated previously, but also to the presence of Me–O–P groups [59], associated to phosphate formation on the metallic surface.

For the treatments at 60 °C, the O1 exhibited a contribution from 52 to 34%, O2 from 53 to 31%, O3 36 to 6% without any specific effect due to whatever the used acidic solution. However, as for P3RT samples, a fourth band, O4 peak, was also detected for 2N60 and 5S60 varying from 8 to 9%. These two conditions also showed the highest O3 values

Table 3
Percentage of area for C1s peaks (C1, C2, C3) and O1s peaks (O1, O2, O3), binding energy (eV) and corresponding chemical groups.

Samples	% of area (C1s peaks)			% of area (O1s peaks)			
	C1 peak	C2 peak	C3 peak	O1 peak	O2 peak	O3 peak	O4 peak
	285.0 eV	286.5 eV	288.5 eV	529.9–530.8 eV	531.7–532.3 eV	533.0–533.7 eV	534.1–534.8 eV
	C–C/C–H	C–O/C–N	C═O-(O-R)	Me–O	Hydroxide/C═O	H_2O/O–C	
AS-REC	55.4	34.7	7.6	46.7	46.0	7.3	–
1CRT	68.7	13.4	17.9	56.8	30.1	13.0	–
1C60	58.0	21.8	20.2	51.9	42.0	6.1	–
2NRT	49.3	37.7	13.0	58.8	32.0	9.3	–
2N60	60.3	21.4	18.4	39.4	30.2	21.9	8.5
3PRT	69.7	24.1	18.4	2.4	67.1	24.1	6.4
3P60	65.2	11.9	22.8	39.4	53.2	7.4	–
4ART	71.8	11.7	16.5	41.7	44.5	13.8	–
4A60	44.7	39.1	16.2	51.5	34.3	14.2	–
5SRT	68.5	19.7	11.7	6.2	71.2	22.6	–
5S60	53.9	33.6	12.4	34.4	20.6	36.1	8.9
6FRT	53.3	31.2	15.4	34.3	56.0	9.8	–
6F60	64.4	19.5	16.1	38.9	41.1	20.0	–

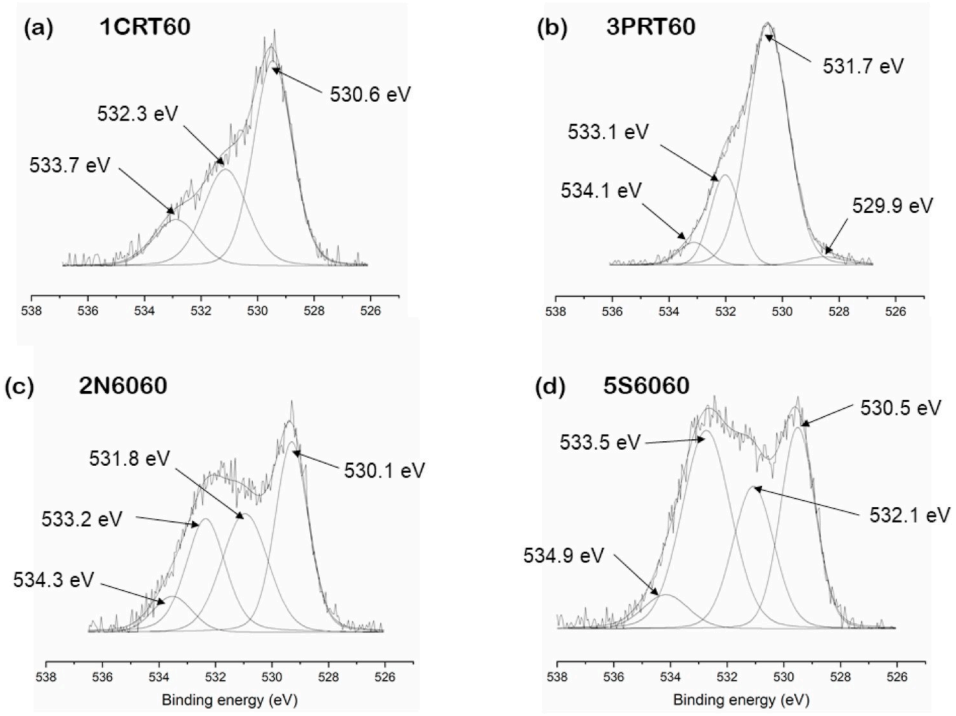

Fig. 7. XPS high-resolution O1s spectra of (a) 1CRT60, (b) 3PRT60, (c) 2N6060 and (d) 5S6060 conditions after acid pickling.

associated with hydrated metal oxides [60].

4. Discussion

Although degradable metallic materials are designed to dissolve within time, the surface properties are of outmost importance to regulate the corrosion and host response of this initial interface between the medical implant and biological environment [14,15,61–67]. Natural and induced oxide layers have been show to increase the surface corrosion resistance and enhance cell compatibility [68,69]. However, scales formed during manufacturing process leads to an uncertain and heterogeneous thick oxide layer with cracks, spallation, porosity and inclusions [70–73]. Removing this manufactured scale and producing a homogeneous oxide layer and controllable surface properties, can be crucial to successful subsequent treatments.

The mechanism of oxide layer removal by acid pickling has been widely investigated for some steel systems [16,18,74]. The main action is the attack of the acid solution of the underlying metal. A large amount of hydrogen can be produced from the dissociation of the acidic solution in contact with elements at the oxide-metal interface and from the reaction itself between the acid and the metallic elements, thus forming molecules in imperfect regions (vacancies, inclusions). Nevertheless, two stages can be observed: the dissolution of the oxide layer, and underlying metal, and its subsequent removal [52].

The character of pickled steel surfaces was described based on mass loss, surface morphologies, cross sectional study, and electrochemical analyses for each acidic solution studied in this work.

4.1. Scale characteristics

Scale in oxidized stainless and carbon steels are assessed in literature: crystalline and classical-three layer could be present [10,75]. Crystalline scale is formed during initial oxidation, while three-layer scale is formed at high temperatures on iron-based substrates. In general, for C steels,

the innermost layer is formed by wüstite (FeO), an intermediate layer by magnetite (Fe_3O_4) and the outmost layer is hematite (Fe_2O_3). The two layers differ by the thickness and the morphology of their scale. A thicker external layer reduces the diffusion of iron, changing the rate-controlling mechanism for the gas/scale interface. Hu et al. [76] investigated the oxide scale growth on high carbon steel (>0.7 wt% C) at high temperatures. It was found that the formed oxide was mainly composed by wüstite and magnetite. Even if the Fe–O equilibrium diagram is expected to form a classical three-layer structure at high temperature, only a low fraction of hematite was detected by laser Raman spectroscopy (LRS) measurements. In the present work, chemical composition of metallic oxides differs from those expected, mainly due to the addition of manganese. For instance, three oxides were observed in the scale composition by XRD: $Mn_{0.43}Fe_{2.57}O_4$, $(FeO)_{0.664}(MnO)_{0.336}$ and Fe_2O_3. No subdivision among the oxides was observed for the cross-sectional areas analyzed by SEM and EDS mapping as mentioned above (Fig. 2).

4.2. Pickling mechanisms: effect on surface properties

4.2.1. Hydrochloric acid

Oxide scale dissolution and removal from a carbon steel matrix showed preferential dissolution of wüstite which is easily dissolved by HCl compared to Fe_3O_4 and Fe_2O_3 Yamaguchi et al. [74] observed that the acid solution dissolves selectively the wüstite portion before achieving the substrate surface. Once a critical crack density is reached, the oxide layer thickness collapses. Therein, two stages could be observed: the formation of cracks in the layer and the following ablation as a consequence of the chemical etching of the substrate [18]. HCl shows the lowest pK_a for the series of acids used in this work (−5.9 to −5.1 from 25 °C to 50 °C) [77]. This is an indicator of the hydrogen production during pickling in chloride solution reacting with metal species (Me), i.e. iron or manganese, according to Eq. (3).

$$x.Me + y.HCl \rightarrow Me_xCl_y + \frac{1}{2}y.H_{2(g)} \quad (3)$$

Regarding the low content of Mn found on the surface for the AS-REC condition (2.8 at.%), the chemical reaction demonstrated in Equation (3) is favored for iron species. From the chemical reactions between iron oxides and hydrochloric acid, metallic chloride ($FeCl_2$) may form [78]. The reaction favoring the formation of this salt must be controlled, to reduce the chemical etching against the base metal and then to avoid an uncontrolled mass loss that could lead to a high-roughness surface [78].

In the present study, time and temperature considerably affected the mass loss of 1C samples, reaching a maximum value when pickled at 60 °C for 240 s. A discontinuity on the trendline of mass loss (Fig. 1) was observed for a range of 100–120 s for 1C conditions at 21 °C and 60 °C. This interval indicates the removal of the oxide layer and the beginning of over-pickling. Considering the mass loss of 1C samples, when compared to the calculated mass of the scale ($m_{oxi} = 0.006$ g), only those pickled longer than 240s at 21 °C are greater than or equal to these values (0.009 g). In opposite, when the same condition is compared to the calculated volume occupied by the scale ($v_{oxi} = 1\%$), a lower volume percentage was found, 0.67%. These findings indicate a lack in the attempt to properly calculate the degree of pickling without considering surface defects such as porosity and their consequent heterogeneous dissolution. Moreover, during the process of pickling morphology, roughness and products produced on the surface contributes to the degree of pickling.

Changes in the surface morphology are shown in Fig. 5 a.1-7, exhibiting cavities with micro cellular aspects that came from the metal/acid/metal dissolution. Some pitting spots could also be observed, indicating an over-pickling of the base material after 60 s. Roughness is shown to mainly vary with time and increase from 0.93 to 1.15 μm by increasing the temperature. However, contact angle exhibited a proportional variation (~20%), decreasing its hydrophobicity. From XPS spectra, 1CRT and 1C60 conditions maintained the same oxygen content with increasing temperature. The high-resolution O1s spectra exhibited mainly three peaks, located at 530.6 eV, 533.3 eV and 534.1 eV as can be seen on Table 3. The first corresponds to metal oxide species, probably oxides from the scale as $Mn_{0.43}Fe_{2.57}O_4$, $(FeO)_{0.664}(MnO)_{0.336}$ and Fe_2O_3. The second peak refers to species such as $Me(OH)_2$ and also MeOOH, such as goethite, where Me corresponds to a metallic element, for example Fe or Mn. The higher binding energy was attributed to adsorbed H_2O [79]. The presence of O^{2-}, OH^- and H_2O are also commonly observed after pickling treatment. In particular, passing from 21 °C to 60 °C, more hydroxide contribution is observed and rather less water adsorption contribution. Moreover, higher contribution of metal oxide species was observed after acid pickling. In fact, the amount of oxygen detected by XPS analyses was significantly higher for 1C samples, tested at both 21 and 60 °C, comparing to that detected for AS-REC samples. However, from the Fe/Mn atomic ratio, a surface enrichment of Fe was observed, especially for the higher temperature condition, 60 °C. The decrease of Mn could be attributed to the scale removal and to the presence of the Mn-depleted layer depicted in Fig. 2 f. These findings corroborate that the different dissolution rates were observed for the mass loss range between 100 and 120 s (Fig. 1 a), indicating then, the beginning of probably over-pickling of the substrate. Increasing the time of treatment up to 60 s allowed the removal of the native oxide layer. The difference in mass loss for 1CRT60 and 1C6060 may be attributed to the pickling of the Mn-depleted layer, since this latter condition presented less manganese amount.

4.2.2. Nitric acid

Nitric solutions are effective in removing metallic contaminations, but not efficient enough to remove scale or heavy deposits of corrosion products [17,30]. Normally, HNO_3 is used in a second pickling treatment, sometimes named as final pickling, where it acts as an agent to promote passivation and the dissolution of oxides remaining on the surface of metallic materials after a first pickling with an acidic solution [17]. The production of nitrates and nitrous gas is the main disadvantage related to the use of this acidic solution [30]. Moreover, the use of nitric solution may induce intergranular corrosion and over-pickling, which can affect the quality of the surface finish [80].

When reacting with iron or manganese, a viscous layer is formed, then NO_3^- combines with the oxide present in the scale and produce NO and water according to Eq. (4).

$$Me + x.HNO_3 \rightarrow Me(NO_3)_x + \frac{1}{2}x.H_2 \quad (4)$$

The pK_a constant for HNO_3 solutions does not highly oscillate with the temperature. Its value is ~ −1.3 from 25 °C to 50 °C [81]. Moreover, by increasing the temperature, the viscosity of the solution decreases, also reducing the diffusion and the degree of the dissociation. As a result, the mechanism of interaction with the metallic substrate may be modified [12]. According to equation (4), nitrate formation is governed by dissociation of nitric acid and reaction of NO_3^- with the substrate. However, another reaction route foresees an adsorption process mechanism where hydroxyl groups react with HNO_3 and form adsorbed nitrate and water [82]. This transition mechanism was evidenced by XPS high-resolution O1s spectra. At 21 °C, 2 N samples exhibited a higher oxide and hydroxide contribution compared to the samples tested in the same solution at 60 °C. Besides, an increase of hydrated metal oxide contribution corresponding to O3 ~ 533 eV peak was found, as well as an emerging fourth peak at 534 eV, from water adsorption, was detected at 60 °C compared to 21 °C. These observations lead to the conclusion that the temperature influenced the mechanism of nitrate formation by dissociation of nitric acid at 21 °C and hydroxyl reaction at 60 °C. In fact, 2NRT samples presented a higher amount of nitrogen compared to 2N60 which is in accordance with the previously discussed mechanism. Afterwards, an amount of 58.8% for the oxide peak at 530 eV was found on

2NRT samples, whereas only 39.4% was detected for 2N60 samples. It may be due to a favorable thermodynamic process promoting the nitrate reaction with Me_2O_3 (i.e hematite) present on the substrate. Even if Fe/Mn ratio for 2NRT condition was the same as that this one calculated for the bulk composition of the substrate (8:1), this phenomenon had no impact on the mass loss (Fig. 1 b) or on the roughness where no significant differences (Fig. 3) were noticed with increasing temperature. In addition, no impact on wettability was observed by increasing the time at 21 °C (Fig. 4).

4.2.3. Phosphoric acid

In general, phosphoric acid is not commonly used to pickle metallic surfaces due to its small content of free protons in an acidic bath [83]. Furthermore, this acid is known to be less effective than the other traditional acid solutions used for pickling processes and is generally employed as a complementary acid in sulfuric and hydrochloric solutions [45]. Heating acid solutions may reduce viscosity and increase the activity by turning the ions more mobile, and then increasing the pickling efficiency [84]. H_3PO_4 presents a pK_a of 2.2 at 25 °C increasing to 2.3 at 60 °C [81]. However, a complex dilution may form different ions (e.g, $H_2PO_4^-$, HPO_4^{2-}, PO_4^{3-}) and react with the substrate according to Eq. (5)

$$x.Me + y.H_3PO_4 \rightarrow Me_x(PO_4)_y + \frac{3}{2}\,y.H_2 \quad (5)$$

From Eq. (5), phosphoric acid is prone to react in aqueous solutions; however the mechanism related to polyphosphates-stainless steel and polyphosphate-carbon steel interaction is still partially unclear, in spite of the fact that has only recently been studied [44,54]. Three main phenomena are assumed: a) polyphosphates are formed in the solution and then adsorbed on the steel surface, b) a polymerization takes place at the solution-substrate interface or c) both situations take place. In the present work, no significant mass loss was observed with varying temperature and time, even though the same temperature ranges from other studies confirmed a noticeable increase in mass loss [46,85] with increasing temperature. The immersing exposition in this study (30 s–60 s) seemed to be insufficient to intensify this phenomenon. SEM images (Fig. 5 c.1) showed the presence of white regions that may be related to polyphosphatization of the surface. The O1s spectra displayed in this study displayed a peak at 531.7 eV that is assigned to hydroxyl-metal compounds, but it overlaps to bands corresponding to P═O, P–O$^-$ and PO_4 contributions. Regarding the P contribution deduced from XPS survey spectra, at 21 °C, a high amount of phosphorous (14 at. %) was detected compared to 60 °C (4.2 at. %), which evidenced that the mechanism of phosphatization is hindered at higher temperatures. This hypothesis is corroborated by the low metallic contribution detected by XPS survey for room temperature conditions: the ratio between Fe/Mn for 3PRT60 sample was 4:1, while for 3P6060, 10:1. Also, the metallic oxides contribution found in O1s high resolutions spectra (Table 3) and corresponding to the peak at 530 eV increased drastically from 2.4% at room temperature to 39.4% at 60 °C for 3P6060. Therewith, all this evidence suggests that at 21 °C phosphates induced a preferential polymerization at the interface of substrate-H_3PO_4 due to the elevated viscosity of the solution, which enhances the substrate dissolution. Otherwise, phosphate adsorption may take place from the interaction with hydrogen bonds. This mechanism is favored by the presence of hydroxyl groups. This was true especially for 3PRT condition, as suggested by Liascukiene et al. [54]. Conversely, by increasing the temperature, a less viscous acidic solution with a higher pK_a is formed. This could promote the increased dissolution of phosphates in solution or decrease proportionally the mechanism at interface. These findings were supported by the Fe/Mn ratio that drastically decreased for 3PRT60 (4:1) compared to the ratio of the bulk material. Moreover, the increase of Fe/Mn ratio observed for 3P6060 (10:1) is not an evidence of scale removal due to the amount of iron (8.5 ± 1.4 at.%) detected by XPS survey analyses, which was statistically the same for the AS-REC condition (6.4 ± 1.5 at.%).

4.2.4. Acetic acid

Acetic acid solutions are widely studied because of their presence in the oil and gas industry [86] They are also known to simulate reactions with metallic substrates for food industry [87] uses. It is considered a weak acid which is only partially dissolved in aqueous solutions (pK_a 2.1 to 2.3 for 25 °C and 60 °C) [88]. Recent studies investigated the corrosion mechanism of mild steel in the presence of acetic acid [89,90]. They suggested that acetic acid does not generate a significant amount of electroactive species, while it mainly increases the mass transfer limit of hydrogen gas formation. Only in specific conditions, e.g. at high temperatures, acetic acid exhibited a high corrosion rate by buffering the H^+ concentration at the metallic surface [89]; furthermore, it was observed that the electrochemical behavior of austenitic steels exposed to acetic acid is mainly dependent on metallic acetates produced from the complexation of acetate ions [91] which allow the dissociation of this solution as shown in Eq. (6):

$$x.Me + y.CH_3CO_2H \rightarrow Me_x(CH_3CO_2)_y + \frac{1}{2}y.H_{2(g)} \quad (6)$$

Although the low mass loss observed for acetic acid pickled samples increasing the temperature the (Fig. 1d). Surface roughness did not present a statistical difference among the investigated conditions (Fig. 2). The pickling process performed in acetic acid solution exhibited less hydrophobic behavior related to the immersion time and temperature (Fig. 4). The surface composition assessed by XPS is also similar at 21 °C or at 60 °C for 60 s of immersion. However, from XPS high resolution of C1s, adsorption of acetic acid was detected [92,93] at higher temperature. Indeed, the C peak at 286.5 eV assigned for the presence of carbon from C–O reached 39% for 4A60 whereas its contribution was only 12% at room temperature (ART60). Also, it should be mentioned that the presence of carboxylates with binding energy between 289.3 and 290.1 eV [94] was not detected for both temperatures, as it could be expected. Indeed, the acetic acid pickling mechanism is described as an adsorption of acetic acid on metallic oxides inducing the breaking of Me–OH bond and the formation of acetate species. Also, a recent study mentions that, due to the higher dissociation of acetic acid at high temperatures, the formation of enolate species could be induced and detected at 286.5 eV [92]. In our case, the formation of acetate or enolate groups on the surface is unclear, since none of them were evidenced in high-resolution spectra of C1s. Regarding O1s high-resolution, once again, the O peak attributed to acetate was not detected (~532.4 eV), which suggests that no acetate is formed in the mentioned conditions. Moreover, the Fe/Mn ratio calculated for 4ART and 4A60 were much lower than that found for the bulk of the material which evidences the change in the chemical composition on the surface, creating a barrier, therefore, obstructing the possibility of the scale removal.

4.2.5. Sulfuric acid

H_2SO_4 is widely used as pickling liquor for carbon steel since it is a cheap acid and presents an efficient pickling behavior [18,95]. The mechanism of oxide scale removal is well known and the main reaction with the metal is given below, Eq. (7):

$$x.Me + y.H_2SO_4 \rightarrow Me_x(SO_4)_y + y.H_{2(g)} \quad (7)$$

As it can be seen, sulfuric acid forms ferrous sulfate, sulfide, water and hydrogen gas with the base metal [18]. The concentration and the bath temperature of a sulfuric acid solution were widely studied and summarized in the ASM metals handbook [18]. Increasing temperature and time improves the dissolution of the steel due to its enhanced reactivity with the surface [95]. H_2SO_4 presents a pK_a of ~2 at 21 °C and ~2.3 at 60 °C [81]. Indeed, the mechanism presented for H_2SO_4 dissolution is dependent of temperature, agitation and concentration [96]. From electrochemical characterization, it was evidenced that the corrosion is essentially controlled by surface reactions. One

disadvantage of sulfuric acid solution is the pitting formation. The pitting probability is a function of the thickness of the oxide layer which may promote concentrate hydrogen formation in the base material without total removal of the oxide scale [30].

In the present study, neither the variation of time, nor temperature showed to affect the weight loss of the 5S samples. Only a discontinuity in the trendline of mass loss (Fig. 1 e) was observed for a range of 15–30s at 21 °C and after 15s at 60 °C which may indicate a peak of dissolution. However, the Fe/Mn ratio decreased for 4:1 for both conditions, indicating an important discrepancy regarding the ratio calculated for the bulk material. Moreover, SEM images (Fig. 5 e.7-8) showed relevant features for 5S6060 that could be related to the higher surface roughness observed for this condition (Fig. 3 b). In fact, after sulfuric acid immersion at room temperature, 5SRT60, a roughness $R_a = 0.77$ μm ± 0.18 μm was obtained with homogeneous morphology (Fig. 5 e.2). A higher roughness, Ra = 0.91 μm ± 0.06 μm, was found for 5S6060. This can be explained by a non-uniform dissolution mechanism which may result in a final rougher surface with observable compact features (Fig. 5 e.8) that may be related to residual oxide on the surface [95]. The hypothesis of the presence of oxidized scale remains, even for higher temperature treatment, is also supported by XPS results. In fact, the high-resolution spectra of O1s evidenced a significant metallic oxide contribution (probably associated to Fe and Mn oxides, peak at 530.8 eV) reaching 34.4% at 60 °C, compared to only 6.2% at 21 °C (Table 3). In addition, when the pickling process is performed at room temperature, 12% of sulfur was detected in survey spectra, whereas at high temperature, its presence became negligible (Fig. 6). This amount of sulfur was further related to the oxygen present in the SO_4^{2-} group. In fact, the main S6RT oxygen peak contribution at 532.2 eV was attributed to the presence of sulfates ($Me_x(SO_4)_y$) reaching 71.2 at. %, compared to 20.6 at. % for S660. In austenitic stainless steels [97], the presence of residual surface sulfur could be associated to a non-spontaneous passivation of the substrate, caused by the interaction with a highly concentrated H_2SO_4 solution. This mechanism of dissolution-precipitation forming a mixed-metal sulfate is limited by mass transport of precipitated ferrous sulfate in solid-state formation, i.e. by the formation of a supersaturated solution [98]. Therefore, the corrosion resistance of carbon steel in sulfuric acid is affected by the formation of this passivating protective layer composed of $FeSO_4$, independently of the steel composition [96]. These evidences are supported by the mass loss invariance for 5SRT and 5S60 samples (Fig. 1e). However, increasing the temperature to 60 °C induced a change regarding the oxygen species formed on the metallic surface: the O peak at 532.2 eV (sulfate group) decreased drastically to 20.6%, the one at 533.5 eV (adsorbed water) increased to 33.6%. A new peak at 534.9 eV was found, and assigned to hydroxides bound at surface $Fe_x(SO_4)_y{\cdot}n.H_2O$ [99]. Then, the hydrophilic behavior found for the condition 5S6030 (Fig. 4) could be explained by the fact that a rich interface in hydroxides is formed on the surface.

4.2.6. Hydrofluoric acid

HF generates H^+ ions and may stabilize the redox potential of the solution. Metal-oxides and hydroxides react with hydrofluoric acid as shown in Eq. (8):

$$Me_xO_y + 2y.HF \rightarrow x.MeF_{2y} + y.H_2O \quad (8)$$

Carbon steels are passivated when in contact with HF and form a fluoride layer in function of the bath temperature [100,101]. The acid dissolution constants for the considered concentration are $pK_a = 3.2$ at 21 °C and 3.4 at 60 °C [83]. Unlike HNO_3, this acid is known to dissolve the previously formed passive films of Fe oxides by complexing Fe^{3+} ions for carbon steels [102–104]. When in contact with oxides, HF dissolves them. Thereafter, fluorides ions react with the substrate alloying elements, like Fe and Mn, until the anionic species F^- has totally reacted; then, reactions with the oxygen ions in the solution begins [105]. However, this explanation for the mechanism of reaction between HF and the substrate is not universally accepted. In recent studies, two main mechanisms have been proposed [106,107]. The first one consists of the reaction between diluted HF and the surface elements. Oxides react with HF and form water, leaving the metallic surface exposed, ready to be later passivated. However, 'pockets' of dilute acid remain at the interface of partly dissolved metal-oxide. Finally, occluded cells are created, consisting of a passivated fluorine scale (for example FeF_2). The second mechanism differs from the first one because of the pocket-corrosion process, finally leading to the formation of hydrated Fe-fluorides.

In the present work, a relevant mass loss was found for treatments at 21 °C and 60 °C, Comparing the mass loss values with the calculated mass for the scale, 6F conditions presented greater or equal dissolution for samples immersed longer than 100 s at 21 °C and higher than 30 s at 60 °C. In fact, Li et al. [23] evidenced a mass loss decrease after 70 s of pickling in HF solution.

From high-resolution XPS analysis of C1s, no significant difference of binding energies was observed for the conditions at 21 °C and 60 °C. Indeed, no peak attributed to the CF_y group, mainly assigned at 290.1 eV, 291.1 eV, 292.7 eV, 294.2 eV and 296.7 eV was detected for all conditions. However, from O1s spectra, mainly the peaks located at 530.2 eV, 531.8 eV were present for conditions at both temperatures. For 6FRT and 6F60, a peak at 533.6 eV and at 533.1 eV were found, respectively; these two peaks can be attributed to oxygen bonding with fluorinated carbon ($O\text{-}CF_x$) [108]. The hypothesis of formation of a fluorine scale could also be sustained by the hydrophobic behavior observed for these conditions [109].

5. Conclusion

The present study assessed the effectiveness of different acid pickling processes applied to a Fe–13Mn-1.2C biodegradable steel on the removal of a heterogeneous oxide scale. In particular, six different acidic media (HCl, HNO_3, H_3PO_4, CH_3COOH, H_2SO_4 and HF), two exposition times (30 s and 60 s), and a specific range of temperature (21 °C–60 °C). The different mechanisms occurring at each metal/solution interface were discussed to evaluate the effectiveness of the process parameters and their effect on the material surface features.

Changes in mass loss, morphology and wettability evidenced the synergic effect of temperature and time. Among all conditions, samples treated in HCl and HF at room temperature presented similar magnitude of mass loss (0.03–0.1 g/cm^2) and similar micrometric morphology, microcellular and cavities aspects. However, 1C60 condition showed the highest mass loss values for the time interval studied on this work (0.03–0.05 g/cm^2). Otherwise, mass loss was lower than 0.010 g/cm^2 for other conditions. Comparing all studied acidic immersions, only 3PRT60 and 4A60-30 and 60 s were smoother than the initial surface state (<1.08 ± 0.20 μm) but no significant roughness influence was observed for all conditions. Moreover, 4A and 5S conditions produced a more hydrophilic surface among all samples, and 5S6030 the most hydrophilic behavior. Besides the different dissolution mechanisms, the ratio Fe/Mn for 1CRT, 1C60, and 3P60 was higher compared to AS-REC samples. Indeed, this observation highlighted an increasing of iron on surfaces pickled in hydrochloric acid and less manganese for those treated in phosphoric acid. Although, 1C and 6F presented the highest mass loss rate, from the point of view of the interface of biomaterial-biological environment, 6P, more specifically showed a rapid passivation. Mostly important, the addition of inhibitors and the use of different concentrations of pure acid diluted in an appropriated solvent might be investigated to suit the industrials needs and assure a finer control of the surface features.

CRediT authorship contribution statement

Letícia Marin de Andrade: Conceptualization, Methodology, Formal analysis, Investigation, Data curation, Writing – original draft, Software, Visualization. **Carlo Paternoster:** Conceptualization,

Methodology, Writing – review & editing. **Pascale Chevallier:** Methodology, Validation, Data curation, Writing – review & editing. **Sofia Gambaro:** Methodology, Validation, Data curation, Writing – review & editing. **Paolo Mengucci:** Methodology, Formal analysis, Investigation, Data curation. **Diego Mantovani:** Resources, Writing – review & editing, Visualization, Supervision, Funding acquisition.

Declaration of competing interest

We hereby declare that this manuscript has not been published and it is not under consideration for publication elsewhere. We have no conflicts of interest to disclose.

Acknowledgements

The authors would like to thank Carolina C. Catanio, M.Sc. Samira Ravanbakhsh, M.Sc. Dimitria B. Camasão, M.Sc. and Clarissa A. Baciu for the much appreciate assistance and useful discussions on protocols and results. This work was partially funded by the Natural Science and Engineering Research Council of Canada, the Fonds de Recherche du Québec sur les Natures et Technologies and the Canada Foundation for Innovation.

References

[1] H. Han, S. Loffredo, I. Jun, J. Edwards, Y. Kim, H. Seok, F. Witte, D. Mantovani, S. Glyn-jones, Current status and outlook on the clinical translation of biodegradable metals, Mater. Today 23 (2018) 57–71, https://doi.org/10.1016/j.mattod.2018.05.018.

[2] B.O. Brien, W. Carroll, The evolution of cardiovascular stent materials and surfaces in response to clinical drivers : a review, Acta Biomater. 5 (2009) 945–958, https://doi.org/10.1016/j.actbio.2008.11.012.

[3] C.M. Campos, T. Muramatsu, J. Iqbal, Y.J. Zhang, Y. Onuma, H.M. Garcia-Garcia, M. Haude, P.A. Lemos, B. Warnack, P.W. Serruys, Bioresorbable drug-eluting magnesium-alloy scaffold for treatment of coronary artery disease, Int. J. Mol. Sci. 14 (2013) 24492–24500, https://doi.org/10.3390/ijms141224492.

[4] F. Witte, A. Eliezer, Biodegradable metals, in: Degrad. Implant Mater, 2012, pp. 93–109, https://doi.org/10.1007/978-1-4614-3942-4_5.

[5] J. He, F.L. He, D.W. Li, Y.L. Liu, Y.Y. Liu, Y.J. Ye, D.C. Yin, Advances in Fe-based biodegradable metallic materials, RSC Adv. 6 (2016) 112819–112838, https://doi.org/10.1039/C6RA20594A.

[6] E. Mouzou, C. Paternoster, R. Tolouei, P. Chevallier, C. Alberto, A. Tuissi, D. Mantovani, CO 2 -rich Atmosphere Strongly Affects the Degradation of Fe-21Mn-1C for Biodegradable Metallic Implants, vol. 181, 2016, pp. 362–366, https://doi.org/10.1016/j.matlet.2016.06.017.

[7] M. Caligari Conti, D. Aquilina, C. Paternoster, D. Vella, E. Sinagra, D. Mantovani, G. Cassar, P. Schembri Wismayer, J. Buhagiar, Influence of cold rolling on in vitro cytotoxicity and electrochemical behaviour of an Fe-Mn-C biodegradable alloy in physiological solutions, Heliyon 4 (2018), https://doi.org/10.1016/j.heliyon.2018.e00926.

[8] S. Loffredo, C. Paternoster, N. Giguère, G. Barucca, M. Vedani, D. Mantovani, The addition of silver affects the deformation mechanism of a twinning- induced plasticity steel: potential for thinner degradable stents, Acta Biomater. (2019), https://doi.org/10.1016/j.actbio.2019.04.030.

[9] L. Mao, L. Shen, J. Chen, X. Zhang, M. Kwak, Y. Wu, R. Fan, L. Zhang, J. Pei, G. Yuan, C. Song, J. Ge, W. Ding, A promising biodegradable magnesium alloy suitable for clinical vascular stent application, Sci. Rep. 7 (2017) 1–12, https://doi.org/10.1038/srep46343.

[10] N. Birks, G.H. Meier, F.S. Pettit, Introduction to the High Temperature Oxidation of Metals, second ed., Cambridge University Press, 2006.

[11] T. Schmidt, J. Abbott, Coronary stents: history, design, and construction, J. Clin. Med. 7 (2018) 126, https://doi.org/10.3390/jcm7060126.

[12] G. Yang, B. Wang, K. Tawfiq, H. Wei, S. Zhou, G. Chen, Electropolishing of surfaces: theory and applications, Surf. Eng. 33 (2017) 149–166, https://doi.org/10.1080/02670844.2016.1198452.

[13] R. Kelton, Study of the surface roughness evolution of pinned fatigue cracks, and its relation to crack pinning duration and crack propagation rate between pinning points, in: ASME 2017 Int. Mech. Eng. Congr. Expo. ASME 2017 International Mechanical Engineering Congress and Exposition, 2017, pp. 1–5. Tampa.

[14] Q. Zhao, J. Wang, C. Yin, P. Zhang, J. Zhang, M. Shi, K. Shen, Y. Xiao, Y. Zhao, X. Yang, Y. Zhang, Near-infrared light-sensitive nano neuro-immune blocker capsule relieves pain and enhances the innate immune response for necrotizing infection, Nano Lett. 19 (2019) 5904–5914, https://doi.org/10.1021/acs.nanolett.9b01459.

[15] P. Zhang, Q. Zhao, M. Shi, C. Yin, Z. Zhao, K. Shen, Y. Qiu, Y. Xiao, Y. Zhao, X. Yang, Y. Zhang, Fe3O4@TiO2-Laden neutrophils activate innate immunity via photosensitive reactive oxygen species release, Nano Lett. 20 (2020) 261–271, https://doi.org/10.1021/acs.nanolett.9b03777.

[16] V. Kuklík, J. Kudláček, Chemical pre-treatment, in: Hot-Dip Galvaniz, Steel Struct., 2016, pp. 17–27, https://doi.org/10.1016/b978-0-08-100753-2.00003-3.

[17] ASTM A380/A380M-13, Standard Practice for Cleaning Descaling, and Passivation of Stainless Steel Parts , Equipment , and Systems, ASTM Copyright, 2015, pp. 1–13, https://doi.org/10.1520/A0380.

[18] R.M. Hudson, ASM Handbook, vol. 5, ASM International, 1994, https://doi.org/10.1016/B978-081551500-5.50022-7.

[19] A.V. Levanov, U.D. Gurbanova, O.Y. Isaikina, V.V. Lunin, Dissociation constants of hydrohalic acids HCl, HBr, and HI in aqueous solutions, Russ. J. Phys. Chem. A. 93 (2019) 93–101, https://doi.org/10.1134/S0036024419010187.

[20] J. Reijenga, A. van Hoof, A. van Loon, B. Teunissen, Development of methods for the determination of pKa values, Anal. Chem. Insights 8 (2013) 53–71, https://doi.org/10.4137/ACI.S12304.

[21] S.A. Rahim, V.P. Muhammad Rabeeh, M.A. Joseph, T. Hanas, Does acid pickling of Mg-Ca alloy enhance biomineralization? J. Magnes. Alloy. 9 (2021) 1028–1038, https://doi.org/10.1016/j.jma.2020.12.002.

[22] E. Vermesse, C. Mabru, L. Arurault, Surface integrity after pickling and anodization of Ti-6Al-4V titanium alloy, Appl. Surf. Sci. 285 (2013) 629–637, https://doi.org/10.1016/j.apsusc.2013.08.103.

[23] L.F. Li, P. Caenen, M. Daerden, D. Vaes, G. Meers, C. Dhondt, J.P. Celis, Mechanism of single and multiple step pickling of 304 stainless steel in acid electrolytes, Corrosion Sci. 47 (2005) 1307–1324, https://doi.org/10.1016/j.corsci.2004.06.025.

[24] A. Verma, A. Choubey, A. Raval, D. Kothwala, Thermal processing and characterization of 316LVM cardiovascular stent, Bio Med. Mater. Eng. 16 (2006) 381–395.

[25] J.Y. Kao, S.Y. Lin, Y.S. Chen, Surface processing technology for 316LVM stainless steel stents, J. Appl. Sci. Eng. 21 (2018) 343–350, https://doi.org/10.6180/jase.201809_21(3).0005.

[26] J. Yang, F. Cui, I.S. Lee, Surface modifications of magnesium alloys for biomedical applications, Ann. Biomed. Eng. 39 (2011) 1857–1871, https://doi.org/10.1007/s10439-011-0300-y.

[27] H. Hermawan, D. Mantovani, Process of prototyping coronary stents from biodegradable Fe-Mn alloys, Acta Biomater. 9 (2013) 8585–8592, https://doi.org/10.1016/j.actbio.2013.04.027.

[28] M.S. Walczak, P. Morales-Gil, T. Belashehr, K. Kousar, P. Arellanes Lozada, R. Lindsay, Determining the chemical composition of corrosion inhibitor/metal interfaces with XPS: minimizing post immersion oxidation, JoVE 2017 (2017) 1–6, https://doi.org/10.3791/55163.

[29] K.F. Khaled, S.S. Abdel-Rehim, G.B. Sakr, On the corrosion inhibition of iron in hydrochloric acid solutions, Part I: electrochemical DC and AC studies, Arab. J. Chem. 5 (2012) 213–218, https://doi.org/10.1016/j.arabjc.2010.08.015.

[30] L.F. Li, J.P. Celis, Pickling of austenitic stainless steels (a review), Can. Metall. Q. 42 (2003) 365–376, https://doi.org/10.1179/cmq.2003.42.3.365.

[31] H.H. Elsentriecy, K. Azumi, H. Konno, Effect of surface pretreatment by acid pickling on the density of stannate conversion coatings formed on AZ91 D magnesium alloy, Surf. Coating. Technol. 202 (2007) 532–537, https://doi.org/10.1016/j.surfcoat.2007.06.033.

[32] ASTM, Standard D7490-13 Standard Test Method for Measurement of the Surface Tension of Solid Coatings, Substrates and Pigments Using Contact Angle Measurements, 2013, https://doi.org/10.1520/D7490-13.2.

[33] A.H. Seikh, E.S.M. Sherif, Effects of immersion time and temperature on the corrosion of API 5L Grade X-65 Steel in 1.0 M H2SO4 pickling solution, Int. J. Electrochem. Sci. 10 (2015) 895–908.

[34] R.M. Hudson, C.J. Warning, Effect of strip velocity on pickling rate of hot-rolled steel in hydrochloric acid, JOM J. Miner. Met. Mater. Soc. 34 (1982) 65–70, https://doi.org/10.1007/BF03339114.

[35] H.F. Staley, The Theory of Pickling of Sheet Iron and Steel for Enameling Proposes, American Ceramic Society, Atlanta, 1926, pp. 787–796, https://doi.org/10.1090/stml/056/02.

[36] H. Rojacz, F. Birkelbach, L. Widder, M. Varga, Scale adhesion, scratch and fracture behaviour of different oxides formed on iron based alloys at 700 °C, Wear 380–381 (2017) 126–136, https://doi.org/10.1016/j.wear.2017.01.004.

[37] T.D. Nguyen, J. Zhang, D.J. Young, Effect of Mn on oxide formation by Fe-Cr and Fe-Cr-Ni alloys in dry and wet CO2 gases at 650 °C, Corrosion Sci. 112 (2016) 110–127, https://doi.org/10.1016/j.corsci.2016.07.014.

[38] G.C. Lecis, C. Lenardi, A. Sabatini, The effect of Mn-depleted surface layer on the corrosion resistance of shape memory Fe-Mn-Si-Cr alloys, Metall. Mater. Trans. A Phys. Metall. Mater. Sci. 28 (1997) 1219–1222, https://doi.org/10.1007/s11661-997-0287-z.

[39] J.M. Oh, Microstructural development in the surface region during oxidation of iron-manganese-nickel-silicon alloys, J. Electrochem. Soc. 133 (1986) 1042, https://doi.org/10.1149/1.2108702.

[40] Y. Kang, K. Han, J.H. Park, C. Lee, Mn-depleted zone formation in rapidly cooled high-strength low-alloy steel welds, Metall. Mater. Trans. A Phys. Metall. Mater. Sci. 45 (2014) 4753–4757, https://doi.org/10.1007/s11661-014-2470-3.

[41] T.E. Society, Kinetics of Oxidation Induced Transformations in Iron - Manganese - Nickel - Silicon Alloys Kinetics of Oxidation Induced Transformations in Iron-Manganese-Nickel-Silicon Alloys, 1987.

[42] V.A. Lashgari, G. Zimbitas, C. Kwakernaak, W.G. Sloof, Kinetics of internal oxidation of Mn-steel alloys, Oxid. Metals 82 (2014) 249–269, https://doi.org/10.1007/s11085-014-9490-7.

[43] I.R. Souza Filho, A. Kwiatkowski da Silva, M.J.R. Sandim, D. Ponge, B. Gault, H.R. Z. Sandim, D. Raabe, Martensite to austenite reversion in a high-Mn steel: partitioning-dependent two-stage kinetics revealed by atom probe tomography,

in-situ magnetic measurements and simulation, Acta Mater. 166 (2019) 178–191, https://doi.org/10.1016/j.actamat.2018.12.046.
[44] M. Ben Salah, R. Sabot, P. Refait, I. Liascukiene, C. Méthivier, J. Landoulsi, L. Dhouibi, M. Jeannin, Passivation behaviour of stainless steel (UNS N-08028) in industrial or simplified phosphoric acid solutions at different temperatures, Corrosion Sci. 99 (2015) 320–332, https://doi.org/10.1016/j.corsci.2015.07.025.
[45] R. Niklasson, R. Nilsson, P. Nobel, A Method of Acid Pickling Iron and Iron Alloys and a Composition for Carrying Out the method.Pdf, WO 81/01298, 1981.
[46] M. Benabdellah, B. Hammouti, Corrosion behaviour of steel in concentrated phosphoric acid solutions, Appl. Surf. Sci. 252 (2005) 1657–1661, https://doi.org/10.1016/j.apsusc.2005.03.191.
[47] J. Drelich, E. Chibowski, D.D. Meng, K. Terpilowski, Hydrophilic and superhydrophilic surfaces and materials, Soft Matter 7 (2011) 9804–9828, https://doi.org/10.1039/c1sm05849e.
[48] S. Becker, R. Merz, H. Hasse, M. Kopnarski, Solvent cleaning and wettability of technical steel and titanium surfaces, Adsorpt. Sci. Technol. 34 (2016) 261–274, https://doi.org/10.1177/0263617416645110.
[49] Q. Liu, Q. Zhang, M. Zhang, F. Yang, K.P. Rajurkar, Effects of surface layer of AISI 304 on micro EDM performance, Precis. Eng. 57 (2019) 195–202, https://doi.org/10.1016/j.precisioneng.2019.04.006.
[50] M. Pantoja, F. Velasco, J. Abenojar, M.A. Martinez, Development of superhydrophobic coatings on AISI 304 austenitic stainless steel with different surface pretreatments, Thin Solid Films 671 (2019) 22–30, https://doi.org/10.1016/j.tsf.2018.12.016.
[51] S. Parvate, P. Dixit, S. Chattopadhyay, Superhydrophobic surfaces: insights from theory and experiment, J. Phys. Chem. B 124 (2020) 1323–1360, https://doi.org/10.1021/acs.jpcb.9b08567.
[52] Y.Y. Yue, C.J. Liu, P.Y. Shi, M.F. Jiang, L.Y. Qin, G.W. Fan, Descaling behavior of 430 hot-rolled stainless steel in HCl-based solution, J. Iron Steel Res. Int. 23 (2016) 190–196, https://doi.org/10.1016/S1006-706X(16)30033-4.
[53] S. Hofmann, Auger- and X-Ray Photoelectron Spectroscopy in Materials Science: A User-Oriented Guide Xps 관련 전자책, 2013, https://doi.org/10.1007/978-3-642-27381-0.
[54] I. Liascukiene, M. Ben Salah, R. Sabot, P. Refait, L. Dhouibi, C. Méthivier, J. Landoulsi, M. Jeannin, Deciphering the role and nature of phosphate species at the surface of stainless steel immersed in phosphoric acid solutions, Appl. Surf. Sci. 434 (2018) 561–572, https://doi.org/10.1016/j.apsusc.2017.10.153.
[55] Y. Wang, X. Liu, H. Wang, G. Xia, W. Huang, R. Song, Microporous spongy chitosan monoliths doped with graphene oxide as highly effective adsorbent for methyl orange and copper nitrate (Cu(NO3)2) ions, J. Colloid Interface Sci. 416 (2014) 243–251, https://doi.org/10.1016/j.jcis.2013.11.012.
[56] H. Li, C. Rameshan, A.V. Bukhtiyarov, I.P. Prosvirin, V.I. Bukhtiyarov, G. Rupprechter, CO2 activation on ultrathin ZrO2 film by H2O co-adsorption: in situ NAP-XPS and IRAS studies, Surf. Sci. 679 (2019) 139–146, https://doi.org/10.1016/j.susc.2018.08.028.
[57] M. Mullet, V. Khare, C. Ruby, XPS study of Fe(II)-Fe(III) (oxy)hydroxycarbonate green rust compounds, Surf. Interface Anal. 40 (2008) 323–328, https://doi.org/10.1002/sia.2758.
[58] R.K. Brow, C.M. Arens, X. Yu, E. Day, XPS study of iron phosphate glasses, Phys. Chem. Glasses (1994).
[59] Q. Xie, Y. Li, Z. Lv, H. Zhou, X. Yang, J. Chen, H. Guo, Effective adsorption and removal of phosphate from aqueous solutions and eutrophic water by Fe-based MOFs of MIL-101, Sci. Rep. 7 (2017) 1–15, https://doi.org/10.1038/s41598-017-03526-x.
[60] S.J. Kerber, J.J. Bruckner, K. Wozniak, S. Seal, S. Hardcastle, T.L. Barr, The nature of hydrogen in x-ray photoelectron spectroscopy: general patterns from hydroxides to hydrogen bonding, J. Vac. Sci. Technol. A 14 (1996) 1314–1320, https://doi.org/10.1116/1.579947.
[61] Y. Shen, M. Gao, Y. Ma, H. Yu, F. zhai Cui, H. Gregersen, Q. Yu, G. Wang, X. Liu, Effect of surface chemistry on the integrin induced pathway in regulating vascular endothelial cells migration, Colloids Surf. B Biointerfaces 126 (2015) 188–197, https://doi.org/10.1016/j.colsurfb.2014.12.019.
[62] W.J. Lin, D.Y. Zhang, G. Zhang, H.T. Sun, H.P. Qi, L.P. Chen, Z.Q. Liu, R.L. Gao, W. Zheng, Design and characterization of a novel biocorrodible iron-based drug-eluting coronary scaffold, Mater. Des. 91 (2016), https://doi.org/10.1016/j.matdes.2015.11.045.
[63] T. Huang, Y. Cheng, Y. Zheng, Biointerfaces in vitro studies on silver implanted pure iron by metal vapor vacuum arc technique, Colloids Surf. B Biointerfaces 142 (2016) 20–29, https://doi.org/10.1016/j.colsurfb.2016.01.065.
[64] T. Huang, Y. Zheng, Y. Han, Accelerating Degradation Rate of Pure Iron by Zinc Ion Implantation, 2016, pp. 205–215, https://doi.org/10.1093/rb/rbw020.
[65] T. Huang, Y. Zheng, Uniform and accelerated degradation of pure iron patterned by Pt disc arrays, Nat. Publ. Gr. (2016) 1–11, https://doi.org/10.1038/srep23627.
[66] A.H. Yusop, N.M. Daud, H. Nur, M. Rafiq, A. Kadir, Controlling the degradation kinetics of porous iron by poly (lactic- co -glycolic acid) infiltration for use as temporary medical implants, Nat. Publ. Gr. (2015) 1–17, https://doi.org/10.1038/srep11194.
[67] N. Mohd, N. Boon, A. Hakim, F. Adibah, A. Majid, H. Hermawan, Degradation and in vitro cell- material interaction studies on hydroxyapatite-coated biodegradable porous iron for hard tissue scaffolds, J. Orthop. Transl. 2 (2014) 177–184, https://doi.org/10.1016/j.jot.2014.07.001.
[68] S. Zhu, N. Huang, L. Xu, Y. Zhang, H. Liu, Y. Lei, H. Sun, Y. Yao, Biocompatibility of Fe – O films synthesized by plasma immersion ion implantation and deposition, Surf. Coating. Technol. 203 (2009) 1523–1529, https://doi.org/10.1016/j.surfcoat.2008.11.033.
[69] G. Gąsior, J. Szczepański, A. Radtke, Biodegradable iron-based materials—what was done and what more can be done? Materials 14 (2021) https://doi.org/10.3390/ma14123381.
[70] H. Utsunomiya, T. Nakagawa, R. Matsumoto, Mechanism of oxide scale to decrease friction in hot steel rolling, Procedia Manuf 15 (2018) 46–51, https://doi.org/10.1016/j.promfg.2018.07.168.
[71] H. Utsunomiya, K. Hara, R. Matsumoto, A. Azushima, Formation mechanism of surface scale defects in hot rolling process, CIRP Ann. - Manuf. Technol. 63 (2014) 261–264, https://doi.org/10.1016/j.cirp.2014.03.022.
[72] N. Yukawa, E. Abe, S. Fujiwara, Thermal properties of oxide scale on surface of work roll in hot rolling mill, Procedia Manuf 15 (2018) 59–64, https://doi.org/10.1016/j.promfg.2018.07.170.
[73] C. Grenier, P. Bouchard, P. Montmitonnet, M. Picard, C. Grenier, P. Bouchard, P. Montmitonnet, M. Picard, Behaviour of oxide scales in hot steel strip rolling, in: 11th ESAFORM Conf. Mater. Form, 2008. Lyon.
[74] S. Yamaguchi, T. Yoshida, T. Saito, Improvement in descaling of hot strip by hydrochloric acid, ISIJ Int. 34 (1994) 670–678, https://doi.org/10.2355/isijinternational.34.670.
[75] V.V. Basabe, J.A. Szpunar, Effect of O2 in heating atmosphere on hydraulic descaling in hot rolling of low carbon steel, ISIJ Int. 48 (2008) 467–474, https://doi.org/10.2355/isijinternational.48.467.
[76] X.J. Hu, B.M. Zhang, S.H. Chen, F. Fang, J.Q. Jiang, Oxide scale growth on high carbon steel at high temperatures, J. Iron Steel Res. Int. 20 (2013) 47–52, https://doi.org/10.1016/S1006-706X(13)60043-6.
[77] A. Trummal, L. Lipping, I. Kaljurand, I.A. Koppel, I. Leito, Acidity of strong acids in water and dimethyl sulfoxide, J. Phys. Chem. 120 (2016) 3663–3669, https://doi.org/10.1021/acs.jpca.6b02253.
[78] M.J.L. Gines, G.J. Benitez, T. Perez, E. Merli, M.A. Firpo, W. Egli, Study of the picklability of 1.8 mm hot-rolled steel strip in hydrochloric acid, Lat. Am. Appl. Res. 32 (2002) 281–288.
[79] A.P. Grosvenor, B.A. Kobe, M.C. Biesinger, N.S. Mcintyre, Investigation of multiplet splitting of Fe 2p XPS spectra and bonding in iron compounds, Surf. Interface Anal. 36 (2004) 1564–1574, https://doi.org/10.1002/sia.1984.
[80] B.S. Covino, J.V. Scalera, T.J. Driscoll, J.P. Carter, Dissolution behavior of 304 stainless steel in HNO3/HF mixtures, Metall. Trans. A. 17 A (1986) 137–149, https://doi.org/10.1007/BF02644450.
[81] R.N. Goldberg, N. Kishore, R.M. Lennen, Thermodynamic quantities for the ionization reactions of buffers, J. Phys. Chem. Ref. Data 31 (2002) 231–370, https://doi.org/10.1063/1.1416902.
[82] C.E. Nanayakkara, P.M. Jayaweera, G. Rubasinghege, J. Baltrusaitis, V. H. Grassian, Surface photochemistry of adsorbed nitrate: the role of adsorbed water in the formation of reduced nitrogen species on α-Fe2O3 particle surfaces, J. Phys. Chem. 118 (2014) 158–166, https://doi.org/10.1021/jp409017m.
[83] W.M. Haynes. CRC Handbook of Chemistry and Physics, 95th ed., CRC Press, 2014.
[84] N.C. for B.I. PubChem, Phosphoric acid (n.d.), https://pubchem.ncbi.nlm.nih.gov/compound/Phosphoric-acid. (Accessed 15 April 2020). accessed.
[85] L. Sena, R.C. Reis, A.A. Monteiro, C. Oliveira, C. Reis, P.L. Silva, Analysis of iron FC 250 microstructure under the effect of phosphoric acid corrosion, Procedia Struct. Integr. 22 (2019) 171–180, https://doi.org/10.1016/j.prostr.2020.01.024.
[86] A. Kahyarian, M. Achour, S. Nesic, CO2 corrosion of mild steel, in: Trends Oil Gas Corros. Res. Technol. Prod. Transm, Elsevier Inc., 2017, pp. 149–190, https://doi.org/10.1016/B978-0-08-101105-8.00007-3.
[87] N. Mazinanian, I. Odnevall Wallinder, Y. Hedberg, Comparison of the influence of citric acid and acetic acid as simulant for acidic food on the release of alloy constituents from stainless steel AISI 201, J. Food Eng. 145 (2015) 51–63, https://doi.org/10.1016/j.jfoodeng.2014.08.006.
[88] H.S. Harned, R.W. Ehlers, The dissociation constant of acetic acid from 0 to 60° centigrade, J. Am. Chem. Soc. 55 (1933) 652–656, https://doi.org/10.1021/ja01329a027.
[89] A. Kahyarian, A. Schumaker, B. Brown, S. Nesic, Acidic corrosion of mild steel in the presence of acetic acid: mechanism and prediction, Electrochim. Acta 258 (2017) 639–652, https://doi.org/10.1016/j.electacta.2017.11.109.
[90] T. Tran, B. Brown, S. Nesic, B. Tribollet, Investigation of the mechanism for acetic acid corrosion of mild steel, Corrosion 70 (2014) 223–229. https://corrosionjournal.org/doi/10.5006/0933.
[91] K. Zuñiga-Diaz, C.D. Arrieta-Gonzalez, J. Porcayo-Calderon, J.G. Gonzalez-Rodriguez, M. Casales-Diaz, L. Martinez-Gomez, Electrochemical behavior of austenitic stainless steels exposed to acetic acid solution, Int. J. Electrochem. Sci. 15 (2020) 1242–1263, https://doi.org/10.20964/2020.02.13.
[92] K. Mudiyanselage, A.K. Burrell, S.D. Senanayake, H. Idriss, XPS and NEXAFS study of the reactions of acetic acid and acetaldehyde over UO2(100) thin film, Surf. Sci. 680 (2019) 107–112, https://doi.org/10.1016/j.susc.2018.10.017.
[93] T. Du, J. Ilegbusi, Synthesis and morphological characterization on PVP/ZnO nano hybrid films, J. Mater. Sci. 39 (2004) 6105–6109.
[94] K. Kim, A. Ford, V. Meenakshi, W. Teizer, H. Zhao, K.R. Dunbar, Nanopatterning of Mn12 -acetate single-molecule magnet films, J. Appl. Phys. 102 (2007), https://doi.org/10.1063/1.2800829.
[95] W. Homjabok, S. Permpoon, G. Lothongkum, Pickling behavior of AISI 304 stainless steel in sulfuric and, Hydrochloric Acid Solutions 20 (2010) 1–6.
[96] Z. Panossian, N.L. de Almeida, R.M.F. de Sousa, G.S. Pimenta, L.B.S. Marques, Corrosion of carbon steel pipes and tanks by concentrated sulfuric acid: a review, Corrosion Sci. 58 (2012) 1–11, https://doi.org/10.1016/j.corsci.2012.01.025.

[97] A. Tamba, N. Azzerri, Anodic pickling of stainless steels in sulphuric acid, J. Appl. Electrochem. 2 (1972) 175–181, https://doi.org/10.1007/BF02354974.
[98] J.R. Kish, M.B. Ives, J.R. Rodda, Anodic behaviour of stainless steel S43000 in concentrated solutions of sulphuric acid, Corrosion Sci. 45 (2003) 1571–1594, https://doi.org/10.1016/S0010-938X(02)00232-9.
[99] S. Seefeld, M. Limpinsel, Y. Liu, N. Farhi, A. Weber, Y. Zhang, N. Berry, Y. J. Kwon, C.L. Perkins, J.C. Hemminger, R. Wu, M. Law, Iron pyrite thin films synthesized from an Fe(acac)3 Ink, J. Am. Chem. Soc. 135 (2013) 4412–4424, https://doi.org/10.1021/ja311974n.
[100] J. Aigueperse, P. Mollard, D. Devilliers, M. Chemla, R. Faron, R. Romano, J. P. Cuer, Fluorine compounds, inorganic, Ullmann's encycl. Ind. Chem. (2012) 398–435, https://doi.org/10.1002/14356007.a11_307.
[101] N. Miki, M. Maeno, K. Maruhashi, Y. Nakagawa, T. Ohmi, Fluorine Passivation of metal surface for self-cleaning semiconductor equipment, IEEE Trans. Semicond. Manuf. 3 (1990) 1–11.
[102] J.L. Gálvez, J. Dufour, C. Negro, F. López-Mateos, Routine to estimate composition of concentrated metal-nitric-hydrofluoric acid pickle liquors, Hydrometallurgy 96 (2009) 88–94, https://doi.org/10.1016/j.hydromet.2008.08.007.
[103] K.M. Österdahl, Å.C. Rasmuson, Solubility of β-FeF3·3H2O in mixtures of nitric and hydrofluoric acid, J. Chem. Eng. Data 51 (2006) 223–229, https://doi.org/10.1021/je050347n.
[104] C. Pedrazzini, P. Giordani, Process for Stainless Steel Pickling and Passivation without Using Nitric Acid, 2000. US006068001A.
[105] G. Zou, W. Shi, S. Xiang, X. Ji, G. Ma, R.G. Ballinger, Corrosion behavior of 904L austenitic stainless steel in hydrofluoric acid, RSC Adv. 8 (2018) 2811–2817, https://doi.org/10.1039/c7ra12453h.
[106] H.P.E. Helle, A proposed mechanism for corrosion of C-steel in trace HF-acid and the effect of residual elements, in: NACE - Int. Corros. Conf. Ser. 2015-Janua, 2015.
[107] X. Chen, L. Yang, H. Dai, S. Shi, Exploring factors controlling pre-corrosion fatigue of 316L austenitic stainless steel in hydrofluoric acid, Eng. Fail. Anal. 113 (2020) 104556, https://doi.org/10.1016/j.engfailanal.2020.104556.
[108] S.-M. Yun, J.-W. Kim, M.-J. Jung, Y.-C. Nho, P.-H. Kang, Y.-S. Lee, An XPS study of oxyfluorinated multiwalled carbon nano tubes, Carbon Lett. 8 (2007) 292–298, https://doi.org/10.5714/cl.2007.8.4.292.
[109] L.J. Hayes, Surface energy of fluorinated surfaces, J. Fluor. Chem. 8 (1976) 69–88, https://doi.org/10.1016/S0022-1139(00)82900-0.